PHILOSOPHICAL TRANSACTIONS OF THE ROYAL SOCIETY A MATHEMATICAL, PHYSICAL & ENGINEERING SCIENCES

Measurement of the Thermal Conductivity of Gases by the Transient Hot-Wire Method

A. I. Johns, A. C. Scott, J. T. R. Watson, D. Ferguson and A. A. Clifford

Phil. Trans. R. Soc. Lond. A 1988 **325**, 295-356
doi: 10.1098/rsta.1988.0054

Phil. Trans. R. Soc. Lond. A **325**, 295–356 (1988) [295]
Printed in Great Britain

MEASUREMENT OF THE THERMAL CONDUCTIVITY OF GASES BY THE TRANSIENT HOT-WIRE METHOD

By A. I. JOHNS[1], A. C. SCOTT[1], J. T. R. WATSON[1], D. FERGUSON[1] and A. A. CLIFFORD[2]

[1] *National Engineering Laboratory, East Kilbride, Glasgow G75 0QU, U.K.*
[2] *Department of Physical Chemistry, University of Leeds, Leeds LS2 9JT, U.K.*

(*Communicated by P. Gray, F.R.S. – Received* 6 *July* 1987)

CONTENTS

Vol. 325. A 1585 [Published 13 June 1988

The construction and operation of an apparatus to measure the thermal conductivity of gases and gas mixtures, by using the transient hot-wire technique, is described. The description is set in the context of the development of this method over the past 12 years in a number of centres and a bibliography of the results obtained in this period is given. The sources of error and the consequences both to the limitations to experimental conditions and to the corrections to be applied are discussed in detail. The experimental and theoretical procedures described are representative of the current state of this developing technique. Results are given for helium and correlating equations given for a data for other gases and gas mixtures. These indicate a precision of 0.1 % and an absolute accuracy of 0.5 % for the apparatus described for temperatures from 300 to 470 K and pressures from 1 to 25 MPa.

0. Nomenclature

A, B	coefficients in equation (2.2)
A	slope of least squares analysis in equation (6.6)
$A(u)$	combination of Bessel functions in equation (5.29)
A_0	area of cross-section of unloaded wire at 0 °C
a	wire radius
a, b, y	resistance ratios in equation (3.6)
a_1, a_2	correlating coefficients in tables 11 and 12
B	intercept of least-squares analysis in equation (6.6)
$B(u)$	combination of Bessel functions in equation (5.30)
b	outer cell radius
C	coefficient in equation (1.9)
$C_t(t)$	temperature correction factor
C_0	height of wire and spring
c_p	specific heat capacity at constant pressure
c_v	specific heat capacity at constant volume

c_v^0	specific heat capacity at infinite volume
d	distance parameter in equation (5.61)
E	Young's modulus
E_1	function defined in equation (1.7)
F	axial force on wire
$[f]_1$	Chapman–Enskog first-order correction to the Eucken factor
$f_\lambda^{(3)}$	third-order correction to thermal conductivity
$f_\eta^{(3)}$	third-order correction to viscosity
g	temperature jump factor in equation (5.47) and acceleration due to gravity
g_n	nth consecutive root of zeroth-order Bessel function
h_0	length of unloaded spring in equation (5.85)
i_1–i_5	currents in resistance network
$J_\nu(u)$	Bessel function of the first kind of order ν
K, L	parameters in equations (5.29) and (5.30)
k	spring constant
k_B	Boltzmann constant
l	length of wire in cell
l_0	length of unloaded wire in equation (5.76)
P	pressure
P_0	constant pressure in equation (5.60)
$Q1, Q2$	integrands in equations (5.36) and (5.37)
q	heat flux per unit length
R	gas constant
Ra	Rayleigh number in equation (5.61)
R_a, R_b, R'	resistances of attenuation chain in Wheatstone bridge
R_{ci}	resistance of R network in Wheatstone bridge
R_L, R_S	resistances of long and short wires
R_T	total resistance in arm of Wheatstone bridge in equation (3.6)
R_1, R_2	variable resistances in Wheatstone bridge
T	temperature
T^*	reduced temperature
T_A, T_B	temperature rises in figure 20
T_0	equilibrium or bath temperature
ΔT	increase in temperature of medium
ΔT_{id}	temperature rise of ideal line source
δT_c	increase in temperature due to convection
δT_K	Knudsen temperature difference
t	time
t_r	time of rth crossover
$\bar{t}$	time before which convection may be neglected in equation (5.67)
t°	standard time in equation (6.6)
u	integration variable in equations (5.27) and (5.28)
V	voltage drop across Wheatstone bridge and volume of container
V_N	effective noise signal
V_c	comparator input noise

PHILOSOPHICAL TRANSACTIONS OF THE ROYAL SOCIETY A MATHEMATICAL, PHYSICAL & ENGINEERING SCIENCES

V_s	signal noise
X	strain on wire
x_t	corrected time in equation (6.6)
$Y_\nu(u)$	Bessel function of the second kind of order ν
y_t	corrected temperature rise in equation (6.6)
α	temperature coefficient of resistance of platinum wire
α_0	local value of α at the equilibrium temperature T_0
β	coefficient of thermal expansion
γ	Euler's constant
δ	axial conduction error
ϵ	error in quantity and Lennard-Jones potential parameter
ϵ_s, ϵ_w	extension of spring and wire
η_0	viscosity at zero density
θ^*	reduced temperature rise for heat capacity
κ	thermal diffusivity
λ	thermal conductivity
λ_t	thermal conductivity in the case of uniform composition in a mixture in equation (5.74)
λ_0	thermal conductivity at zero density
λ_∞	thermal conductivity in the case of the steady state in a mixture in equation (5.74)
ν	Poisson's ratio
ρ	density
σ	wire resistance per unit length
σ_B	Stefan–Boltzmann constant
τ	parameter defined by equation (5.2)
ϕ, χ, χ'	parameters in equations (5.54), (5.55) and (5.57)
ω	twice the ratio of (specific heat × density) products for the fluid and wire defined in equation (5.33)

subscripts

e	experimental
f	fluid or gas
m	measured value
nom	nominal value
r	reference value
s	spring
T	at temperature T
th	theoretical
w	wire
0	at 0 °C
1 or L	long wire
2 or S	short wire

1. The transient hot-wire method

(a) *Introduction*

The thermal-conductivity coefficient of gases at moderate or elevated pressures is required in many important design calculations pertaining to energy transfer (Assael *et al.* 1978). Strong industrial interest has been expressed in the need for methods to predict the thermal conductivity of binary and multicomponent mixtures containing one or more polar components (Assael *et al.* 1978; Cousins & Butterworth 1979). Data surveys (Sutton 1969, 1976) have shown that there is a complete absence of published results for this class of mixture (which includes most mixtures of interest to industry) at pressures greater than atmospheric on which to develop new, or test existing, prediction methods.

With the above-mentioned points in mind, the Properties of Fluids Section at the National Engineering Laboratory, in close cooperation with the Department of Physical Chemistry at Leeds University, began a programme of work in 1976 on the development of a transient hot-wire apparatus for the measurement of gas-phase thermal conductivities in the temperature range 25–300 °C and the pressure range 0–40 MPa. The transient hot-wire method was adopted because recent advances in electronic techniques have helped to establish the method as one of the most accurate ways of determining gas-phase conductivities (Haarman 1969; de Groot *et al.* 1974). The advantage of the method lies firstly in its almost complete elimination of the effects of natural convection, whose unwanted presence presents problems for measurements made with a steady-state apparatus. A second advantage is that physical dimensions of the apparatus, apart from the length of the wire, are not involved in the zeroth-order calculation to the thermal conductivity. This transient hot-wire apparatus is now widely used and the present paper attempts to describe in detail the development and operation of a particular example. Although the apparatus is under continual development, in this laboratory as elsewhere, a full record of the experimental procedure and problems seems worthwhile in view of the large amount of data the method has produced.

(b) *Historical survey*

The transient hot-wire method was first reported by Stalhane & Pyk (1931), who used the technique to measure the thermal conductivity of powders. After 1945 the method was used for liquids by Van der Held & Van Drunen (1949) and again by Gillam & co-workers in 1955. The accuracies of these investigations were all limited to 2%, mainly reflecting the limitations of the systems used to record the transient temperature rise. The position is worst for gases, where the onset of convection occurs at much shorter times than for liquids. Briggs (1965) and Picot (1969) have demonstrated the difficulty of obtaining an accurate recording of the temperature rise as a function of time with a deflection method (e.g. an oscilloscope or deflection galvanometer).

In 1969, Haarman constructed a gas-phase apparatus for low-pressure measurements, with an automatic Wheatstone bridge and electronic timers. With this improved practical system he obtained accuracies of between 0.5–1.0% in the thermal conductivities of helium, argon, krypton, nitrogen and carbon dioxide over a temperature range of 55–195 °C. Following this, de Groot *et al.* (1974) at Brown University constructed a more elaborate version of the hot-wire apparatus with two wires to eliminate end effects. This has subsequently been used to measure the thermal conductivities of the monatomic gases over the pressure range of 1–30 MPa at

room temperature (de Groot *et al.* 1978). Other authors have also applied the technique to solids (Andersson & Backström 1976), and liquids (de Castro 1977; Horrocks & McLaughlin 1963; Mani 1971; McLaughlin & Pitman 1971). For a review of transient hot-wire methods up to 1975 the reader is referred to the paper by Shpil'ran *et al.* (1975).

Table 1 lists the papers on transient hot-wire measurements of both gases and liquids that have appeared in the literature from 1974 up to 1986. The table is organized in chronological order with columns for author, substances measured, temperature and pressure ranges covered, physical state of the fluid (i.e. gas (g) or liquid (l)) and stated accuracy. By 1978 both the electronic instrumentation and the theory of the working equations had developed sufficiently to make the transient hot-wire method the most accurate means of obtaining thermal conductivities, and this is reflected in the steady flow of results for fluid systems from several centres that have developed this method. The main centres are listed with the principal investigators below:

Imperial College, U.K.,	Wakeham,
Brown University, U.S.A.,	Kestin,
National Engineering Laboratory, U.K.,	Watson & Clifford,
National Bureau of Standards, U.S.A.,	Roder,
Universitat Tecnico Superior, Portugal,	de Castro,
Keio University, Japan,	Nagashima & Nagasaka,
University of New Brunswick, Canada,	Venart.

The experimental techniques are divided between single-wire and two-wire systems. In the single-wire case, potential tappings are attached to the wire that measure the change in voltage developed across it during the transient. The voltage is then sampled at known time intervals. The two-wire systems, of which this paper describes one version, do not usually require potential leads.

The apparatus developed at the National Engineering Laboratory (NEL) has so far been used to measure the thermal conductivity in the domain 25–200 °C and 1–25 MPa for (*a*) a number of pure gases, argon and helium (Johns *et al.* 1983), hydrogen and nitrogen (Clifford *et al.* 1981), carbon dioxide (Scott *et al.* 1983); and (*b*) binary mixtures, dry carbon dioxide-free air (Scott *et al.* 1981) and carbon dioxide–nitrogen (Johns *et al.* 1988). Agreement with the results of Brown University and Imperial College is excellent and well within the combined uncertainty limits.

(*c*) *General description of method*

The method is based on the practical realization of the mathematical model of an infinitely long and thin, continuous line source of heat, of flux q per unit length applied as a step at time, $t = 0$. This line source is considered to lose heat by conduction alone into an infinite, incompressible medium of thermal diffusivity κ_t, and thermal conductivity λ_t, increasing the temperature of the medium as time progresses.

In practice, the line source consists of a thin, taut platinum wire (typically 7 μm in diameter) of finite length, which is heated by the application of a voltage step across its ends. The temperature history of the wire is followed as a function of time over a short interval (usually about 1 s for gases). The temperature rise of the wire is given by the change in its electrical

resistance as the experiment progresses, the resistance at a specified time being measured with an automatic Wheatstone bridge.

It can be shown that a plot of the temperature rise, ΔT, of the wire at various bridge balance-points against the natural logarithm of the times of balance will approximate to a straight line, whose slope is $q/4\pi\lambda_t$. From the measured slope and heat generated per unit length, the thermal conductivity can be directly determined. In practice two thin wires of different lengths, l_1 and l_2 are used to avoid end effects, and it is the central section of the long wire that is in effect being studied, as shown in figure 1. For this method to be accurate the end geometries of the two wires must be closely matched.

To illustrate the basic principles of the apparatus, a schematic circuit is shown in figure 2. The two thin wires R_L and R_S, of different lengths, are positioned as arms of a Wheatstone bridge. The other two reference arms consist of known resistors R_A, R_B, and a resistor R_C in parallel with R_A via the reed relay S. Another resistor is also shown that can be connected in parallel with R_A. (In practice there are usually several such resistors.) The output from the bridge is monitored by the comparator C. The sequence of events during an experiment is as follows.

(*a*) The apparatus is energized by applying a suitable voltage V, at time $t = 0$, between points A and B. Simultaneously a timer is started.

(*b*) The wires heat up, bringing the bridge into balance (it being deliberately unbalanced in the initial equilibrium state).

(*c*) As the bridge goes through balance, the polarity change of the comparator turns off the first timer and at the same instant switches in the resistor R_C, unbalancing the bridge once more and starting a second timer.

(*d*) Sequence (*b*) to (*c*) may be repeated for each resistor parallel to R_A.

The effective resistance of the central section of the wire $R_w = (R_1 - R_2)$ at bridge balance, can be computed from the known resistors R_A, R_B, and the known value of R_C in parallel with R_A at the time of balance. From the temperature coefficient of resistance for the wire, the temperature rise of the effective wire at a time t (given by the timers), can be obtained very accurately.

(*d*) *The ideal continuous line source*

The conduction of heat from an infinitely long and thin, continuous line source is governed by the simplest form of the Fourier equation

$$\partial T/\partial t = \kappa_t \nabla^2 T. \tag{1.1}$$

If we assume that for $t \leqslant 0$ the medium is at a uniform temperature T_0 and $T = T_0 + \Delta T_{id}$ the solution will be subject to the boundary conditions, $t \leqslant 0$ and at any r,

$$\Delta T_{id}(r, t) = 0, \tag{1.2}$$

and $t \geqslant 0$ and $r = 0$, $$\lim_{r \to 0} \{r(\partial T/\partial r)\} = -q/2\pi\lambda_t, \tag{1.3}$$

and $t \geqslant 0$ and $r = \infty$, $$\lim_{r \to \infty} \{\Delta T_{id}(r, t)\} = 0. \tag{1.4}$$

The thermal diffusivity of the medium, κ_t, is defined by

$$\kappa_t = \lambda_t/\rho_t c_{p,t}, \tag{1.5}$$

where ρ_t is the density and $c_{p,t}$ the specific heat at constant pressure of the medium.

TABLE 1. EXPERIMENTAL TRANSIENT HOT-WIRE MEASUREMENTS ON FLUIDS SINCE 1974

year (author)	systems	state (gas or liquid)	T range / K	P range / MPa	accuracy (%)
1974					
de Groot *et al.*	He	G	300	1–35	0.2
Takizawa *et al.*	water	L	273–373	0.1–48.7	1.5
1975					
de Castro *et al.*	*n*-heptane	L	293–303	0.1	1.0
Venart & Mani	R12	G, L	300–400	0.2–20	2.0
1976					
de Castro *et al.*	*n*-heptane	L	288–293	0.1	1.0
1977					
Julia *et al.*	water, toluene	L	273–353	0.1	0.3
de Castro (thesis)	toluene dimethylphthalate, heptane, octane, decane	L	283–333	0.1	1.0
de Castro *et al.*	toluene dimethylphthalate and *n*-heptane	L	288–323	0.1	0.5
Sookiazian (thesis)	He, Ar, Kr, Xe, Ar+Ne+Kr, N_2, CH_4, CF_4, CO_2	G	300	0.3–34	0.2
Trump *et al.*	H_2O, methanol, CCl_4, toluene	L	298–313	0.1	1.0
1978					
de Groot *et al.*	He, Ne, Ar, Kr	G	300	0.8–35	1.5
Takizawa *et al.*	H_2O, methanol, ethanol, benzene, acetone, glycerin, R11, R113	L	183–353	0.1	1.5
Parsons & Mulligan	Air	G	296	0.1	1.0
1979					
Clifford *et al.* (*a*)	He+Ar, Ne+Ar, Ne+Ar+Kr	G	300	0.5–15	0.2
de Castro *et al.*	*n*-octane	L	288–333	satn	0.4
Clifford *et al.* (*b*)	N_2, CO_2, CH_4	G	300	0.1–35	0.2
1980					
Clifford *et al.* (*c*)	H_2, D_2, H_2+D_2	G	300	2–36	0.2
Kestin *et al.*	He, Ar, Kr, Ne, Xe	G	300	0.1–35	0.2
Clifford *et al.* (*a*)	H_2+He	G	300	0.1–14	0.2
Baryshev *et al.*	perfluoropropane	G, L	260–430	0.1–60	3.0
Assael & Wakeham	H_2+monatomic gases	G	308	2–9	0.2
Dietz *et al.*	toluene, H_2O	L	298–371	8–100	0.6
Venart *et al.*	D_2O, H_2O	L	273–370	satn	0.5
Fleeter *et al.*	ethane, ethylene, nitrous oxide, air, argon-free air	G	300	0.6–36	0.2
1981					
Scott *et al.*	air	G	312–373	0.1–24	0.5
Clifford *et al.*	Ar, N_2, H_2	G	300–400	0.1–25	0.5
Menashe & Wakeham	*n*-heptane	L	302–348	50–500	0.5
Hoshi *et al.*	heat-transfer salt	L	457–580	0.1	3.5
Vilcu & Ciochina	toluene, CCl_4	L	303–323	0.1	1.5
Fleeter *et al.* (*b*)	He+CH_4	G	300	1–13	0.2
Assael *et al.*	He, Ar, Ne, Kr, Xe, He+Ne, Ar+Kr	G	300	0.5–20	0.2

PHILOSOPHICAL TRANSACTIONS OF THE ROYAL SOCIETY A MATHEMATICAL, PHYSICAL & ENGINEERING SCIENCES

TABLE 1 (*cont.*)

year (author)	systems	state (gas or liquid)	T range / K	P range / MPa	accuracy (%)
1981					
Kitazawa & Nagashima	R11, R113, toluene	L	212–353	0.1–54	1.6
Nagasaka & Nagashima (*b*)	toluene, *n*-heptane	L	273–363	0.1	0.5
Fleeter *et al.* (*a*)	N_2+He, N_2+Ar, N_2+Ne, N_2+Kr	G	300	0.9–17	0.3
Perkins *et al.*	toluene	L	298	0.1	1.1
Nagasaka & Nagashima (*c*)	electrolyte solution	L	273–313	0.1	0.5
Assael & Wakeham	4 polyatomic gases	G	308	0.8–10	0.2
Serbanescu *et al.*	*n*-heptane	L	302–323	0.1	2.0
Roder	He, Ar, N_2	G	300	0.1–70	1.5
de Castro & Roder	Ar	G	298	0.1–68	1.0
1982					
Kestin *et al.* (*c*)	CO_2+He, CO_2+Ne, $Ar+CO_2$	G	300	0.7–11	0.3
Kestin *et al.* (*b*)	H_2+N_2	G	300	0.7–10	0.3
Haran & Wakeham	Ar	G	308–337	0.1–12	0.3
Roder & de Castro	propane	L	111–300	0.1–68	1.5
Kestin *et al.* (*a*)	N_2+CH_4	G	300	0.1–8	0.3
Omotani *et al.*	KNO_3+NaNO_3	L	498–593	0.1	3.0
Fleeter *et al.*	CH_4+Ar, CH_4+Ne	G	300	1–22	0.3
Kashiwagi *et al.* (*b*)	14 liquids	L	298–373	0.1	2.0
Roder	O_2	L, G	278–310	0.1–70	1.5
Kashiwagi *et al.* (*a*)	toluene	L	272–373	0.1–250	1.0
Mustafa *et al.*	*n*-tridecane	L	308–346	20–500	0.7
Alloush *et al.*	$LiBr+H_2O$	L	297–357	0.1	3.0
Vilcu *et al.*	Ar	G	299.8	0.1	2.0
Menashe & Wakeham (*b*)	nonane, undecane	L	308–363	0.1–500	0.3
1983					
Haran *et al.*	Ar, CO, N_2	G	300–430	0.1–10	0.3
Scott *et al.*	CO_2	G	300–348	0.1–25	0.5
Perkins (thesis)	dimethylphthalate, toluene, *m*-xylene, tetrahydronaphthalene, 1-methylnaphthalene, methylcyclohexane, decahydronaphthalene	L	298–675	0.1–14	1.0
Calado *et al.*	*n*-octane, *n*-nonane, *n*-undecane, isooctane, *n*-tetradecane	L	282–373	satn	1.5
Mardolcar & Wakeham	CS_2	L	309–347	0.1–500	0.5
de Castro *et al.*	toluene	L	308–363	0.1–600	0.3
Johns *et al.*	Ar, He	G	300–400	0.1–25	0.5
Ciochina & Vilcu	Ar, N_2, O_2, H_2, CO_2	G	295–300	0.1	2.0
Kestin *et al.*	CH_4+CO_2	G	300	0.1–12	0.3
Nagasaka *et al.*	$NaCl+H_2O$	L	273–353	0.1–40	0.5
1984					
Omotani & Nagashima	$LiNO_3+NaNO_3$	L	531–566	0.1	3.0
Nagasaka *et al.*	$KCl+H_2O$	L	298–473	0.1–50	0.3
Prasad *et al.*	CH_4	G, L	120–400	2.5–70	1.0
Roder (*b*)	*p*-H_2	G	100–275	0.1–12	1.5
Imaishi & Kestin (*b*)	Ar+CO, He+CO, Kr+CO	G	300	0.7–12	0.3
Yata *et al.*	R11, R12, R13, R13b1, R22, R113, R114, R115, R114b2, R124	L	204–450	satn	1.5
Li *et al.* (*a*)	*n*-hexane, *n*-octane	L	308–363	0.1–640	0.3

PHILOSOPHICAL TRANSACTIONS OF THE ROYAL SOCIETY A MATHEMATICAL, PHYSICAL & ENGINEERING SCIENCES

TABLE 1 (*cont.*)

year (author)	systems	state (gas or liquid)	T range / K	P range / MPa	accuracy (%)
1984					
Imaishi *et al.* (*a*)	CO_2+N_2O, N_2+CO	G	300	0.1–12	0.3
Song & Yu	emulsion of kerosine with water	L	298	0.1	2.0
Roder (*a*)	*n*-H_2	G	78–310	0.1–70	1.5
Li *et al.* (*b*)	benzene, cyclohexane	L	309–363	0.1–330	0.3
Prasad & Venart	ethane	G	290–600	0.1–700	0.7–3.0
Bootle *et al.*	oils and fats	L	298	0.1	
Imaishi & Kestin (*a*)	$CO+CH_4$	G	300	0.1–12	0.3
Fareleira *et al.*	branched alkanes	L	309–361	0.1–600	0.3
Richmond *et al.*	lubricants under pressure	L			
1985					
Kestin & Imaishi	SF_6	G	300	0.8–2.2	0.5
Imaishi *et al*	$Ar+CF_4$, $He+CF_4$	G	300	0.1–12	0.4–0.7
Mardolcar *et al.*	Ar	G	329–435	0.1–6	1.7
Knibbe	toluene, heptane	L	287–444	satn	2.0
Glatzmaier & Ramirez	glycerin	L	295–347	satn	1.0
Kawaguchi *et al.*	toluene	L	298.15	0.1	1.5
Roder	CH_4	G, L	110–310	0.1–70	1.6
Roder & de Castro	ethane	G, L	110–325	0.1–70	1.6
Friend & Roder	CH_4 + ethane	G, L	critical region		1.6
Wada *et al.*	C_{11}, C_{14}, C_{15}, C_{16}, paraffins $C_7+C_{11}+C_{16}$, mixture	L	293–363	0.1	1.0–1.5
1986					
Roder & Friend	CH_4 + ethane	G	140–330	0.1–70	1.6
Palavra *et al.*	CCl_4	L	310–364	0.1–220	0.3
Johns *et al.*	Ar, CO_2, N_2	G	300–470	0.1–25	0.5
Maitland *et al.*	He, Ne, Ar, CO_2	G	300–425	0.1–10	0.3
Mardolcar *et al.*	Ar	G	107–423	0.1–9.57	0.5
Nagasaka *et al.*	pentaerythritol	L			
1988					
Johns *et al.*	CO_2+N_2	G	320–470	0.1–25	0.5

The solution to this problem is given by Carslaw & Jaeger (1959) and is as follows.

$$\Delta T_{id}(r,t) = (q/4\pi\lambda_t)\, E_1(r^2/4\kappa_t t), \tag{1.6}$$

where

$$E_1(x) = \int_x^\infty x^{-1} \exp(-x)\, dx, \tag{1.7}$$

and q is the heat dissipated per unit length of the line source.

The exponential integral in (1.7) can be calculated by expressing the integrand as a McClaurin series and integrating term by term. For values of x small compared with unity it is sufficient to retain only the first two terms. (For the experiments described below x is always very much less than unity.) Thus to a very good approximation the solution becomes

$$\Delta T_{id}(r,t) = (q/4\pi\lambda_t) \ln\left(\frac{4\kappa_t t}{r^2 C}\right), \tag{1.8}$$

where

$$C = \exp\gamma, \tag{1.9}$$

and $\gamma = 0.5772\ldots$ is Euler's constant.

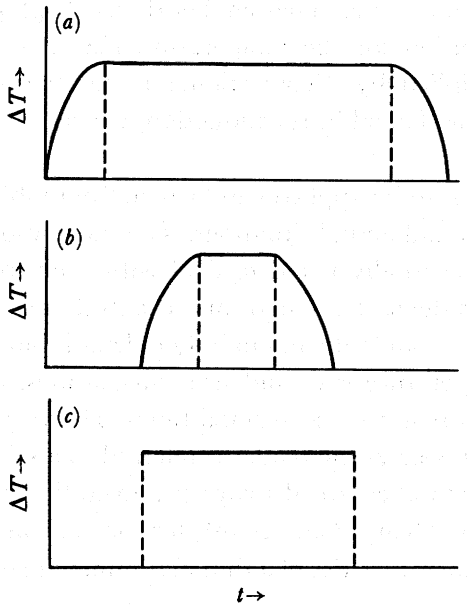

FIGURE 1. Temperature distributions along wires at time t for (a) long wire, (b) short wire and (c) effective wire.

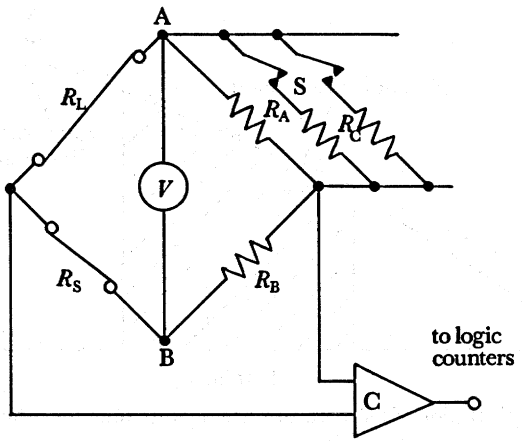

FIGURE 2. Simplified bridge circuit.

Inspection of (1.8) shows that a graph of the temperature rise of the medium at a radial distance r from the line source, against the natural logarithm of the time, is indeed a straight line of slope $q/4\pi\lambda_t$ from which the thermal conductivity of the medium λ_t can be obtained directly.

(*e*) *Corrections to the ideal model*

At first glance it would seem unlikely that in practice a thin platinum wire would follow (1.8) very closely. However, provided certain design criteria are met and a small number of corrections applied, the equation can provide a basis for the precise determination of thermal conductivity coefficients. The philosophy of calculating the degree of approximation to the ideal case is to consider each source of possible error separately as a perturbation of the ideal situation. In some cases it can be shown that the effect on the final result is negligible compared

with the precision of the experiment (i.e. much smaller than 0.1 %) under certain experimental conditions. In others the solution for the temperature rise is given the form of the ideal temperature rise, ΔT_{id}, multiplied by a correction for that particular source of error. An exception to this is the problem of axial heat conduction, which is described in detail in a later section.

The origins of the corrections to be applied can be seen from table 2, which summarizes the differences between the model and actual situations. The table also shows by means of a code the practical steps that are eventually taken to deal with each source of error. The largest corrections, labelled 2 and 4 in the table, stem from the facts that the platinum wires that make up R_L and R_S of figure 2 (*a*) are not identical, not only in length but in other respects, and thus exhibit slightly different temperature rises and heat dissipations, and (*b*) have a finite heat capacity that modifies the temperature rise at small times. The various problems are discussed in detail in §5, although in some cases the reader is referred to a relevant source where further details are given. Much of the mathematical treatment given there follows closely the modern account of the theory given by Healy *et al.* (1976), for most of the problems considered.

Figure 3 shows how the temperature rise of a thin platinum wire deviates from the ideal-line-

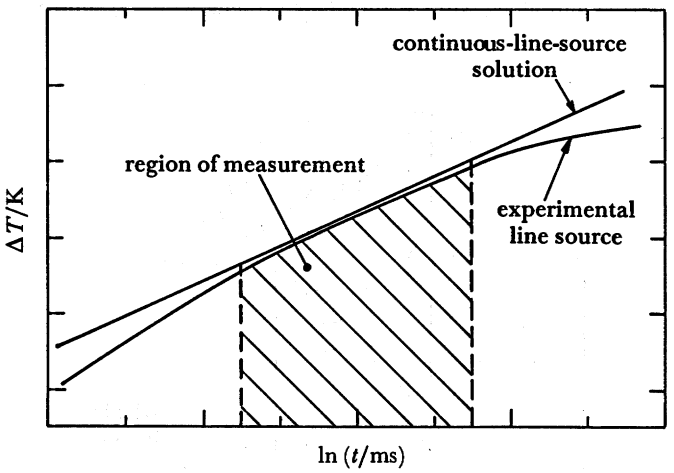

FIGURE 3. Typical plot of temperature rise against time for a hot-wire experiment.

TABLE 2. DIFFERENCES BETWEEN IDEAL AND REAL SITUATIONS IN A HOT-WIRE CELL

	ideal line source	real hot-wire line source	code
1	zero radius, $r = 0$	finite radius, $r = a$	N
2	infinite lengths, $l = \infty$ no end effects	finite length, $l = l_1$ end effects	C D
3	infinite thermal conductivity $\lambda_w = \infty$	finite thermal conductivity λ_w = constant	N
4	zero heat capacity $C_{p,w} = 0$	finite heat capacity $C_{p,w}$ = constant	C
5	infinite medium	cell boundary at $r = b$	C
6	continuous radial temperature profile from axis of source	temperature discontinuity at wire/medium interface at $r = a$	N
7	incompressible medium – constant physical properties	compressible medium – variable physical properties	C
8	conduction as the only mode of heat transfer	radiation contribution + convection at long times	N D

Code: C = corrected for; N = neglected; D = avoided by design.

source solution. At small times the temperature rise is less than that of the ideal case because of the finite heat capacity of the wire. At long times the temperature rise is also less than that of the ideal case: firstly because of the effect of the finite outer boundary of the cell, and secondly, at even longer times, because of natural convection. The central portions of the curves are close, however, and it is this region that is utilized in the transient hot-wire method.

2. Hot-wire cells

(*a*) *Construction*

The cells are shown schematically in figure 4. A are the cell ends and B the two halves that form the walls of both cells, all of which are made of stainless steel (ANSI 316). The inside diameter of the cells is 15 mm and their overall internal length is 210 mm. C are the wire

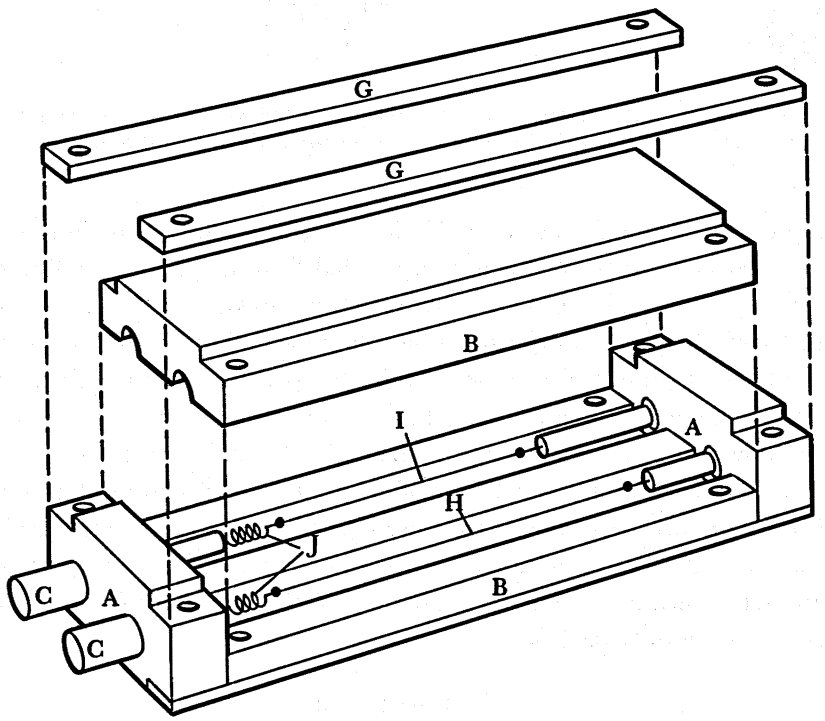

Figure 4. A schematic exploded diagram of the thermal conductivity cells. A are the cell ends. B are the two halves that form the cell walls. C are the wire mountings (shown in figure 5), G the end spacers, H the long wire, I the short wire and J the tensioning springs.

mountings which are shown in detail in figure 5. They consist of a stainless steel outer, D, and 'Macor' inserts, E, through which a gold wire, F, passes and is trapped by a tortuosity in the lead-through holes. Figure 5 shows schematically the mounting for the short wire; the mounting for the long wire is similar in design. The spacers, G in figure 4, are made of stainless steel and define the length of the cell. H represents the long wire (160 mm) and I the short wire (70 mm) both of 7 μm diameter annealed platinum wire (Sigmund Cohn Corp.). J are the tensioning springs. Gas enters and leaves the cell through spaces between the components A and B. Because the platinum wire is so delicate these spaces were kept small to prevent rapid movement of fluid around the wire, which would cause it to work harden and eventually snap.

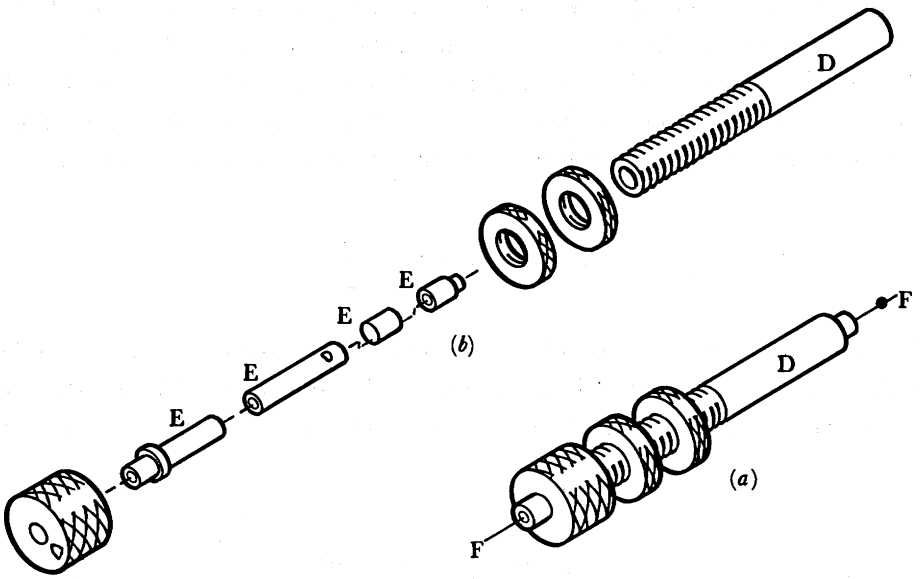

FIGURE 5. A schematic diagram (*a*) assembled and (*b*) exploded of the wire mountings. D are the stainless steel outers, E the ceramic inserts and F the ends of the gold wire, which pass through the mountings.

Figure 6 shows a section of the assembled cell, E, with the long and short wires, F and G, in the pressure vessel. The assembled cell is suspended from a spherical ball and socket joint, D, which ensures that the cell hangs vertically inside the pressure vessel, which in turn implies verticality of the wires. The cell hangs from a flat plate located on the top of a cylindrical liner, H, which is a snug fit in the pressure vessel. The temperature of the cell is measured by a platinum resistance element, which is inserted into a well, I, let in from the pressure vessel cap, B. The cap also allows for eight electrical lead-throughs, K, and a gas inlet connection, A. The main seal, J, consists of a stainless-steel ring of C-shaped cross section. There is another gas connection, A, in the main body, C, which is used as the exhaust. The electrical lead-through is shown in figure 7 and it is usable up to 980 °C. The assembled pressure vessel with cells is placed in an air-bath thermostat. The bath operates in the temperature range 25–300 °C and has a long-term stability of ± 0.01 K.

(*b*) *Wire tension*

The most intricate parts of the apparatus, and the most vital for accurate results, are the platinum filaments. The quality of the results obtained depends markedly on several factors: (*a*) the tautness of the assembled wire; (*b*) the quality of the joints at the wire ends; and (*c*) the ability to define the actual resistance per unit length of the wire (not including the leads). The first of these problems is discussed below and the last two in the next section.

In the transient hot-wire experiment for gases it is necessary to maintain the wires, which are typically made of fine platinum wire of 7 μm diameter, straight and under slight tension. This is achieved in the various apparatuses that have been built by using weak springs or weights or both; in the case of the NEL apparatus by springs. The springs must be designed to keep the wires under tension without stretching them when the wires and the cells, in which they are held, expand thermally by different extents. Two factors must be taken into consideration in the design of a spring. Firstly the wires, but not the cells, expand during the measurement

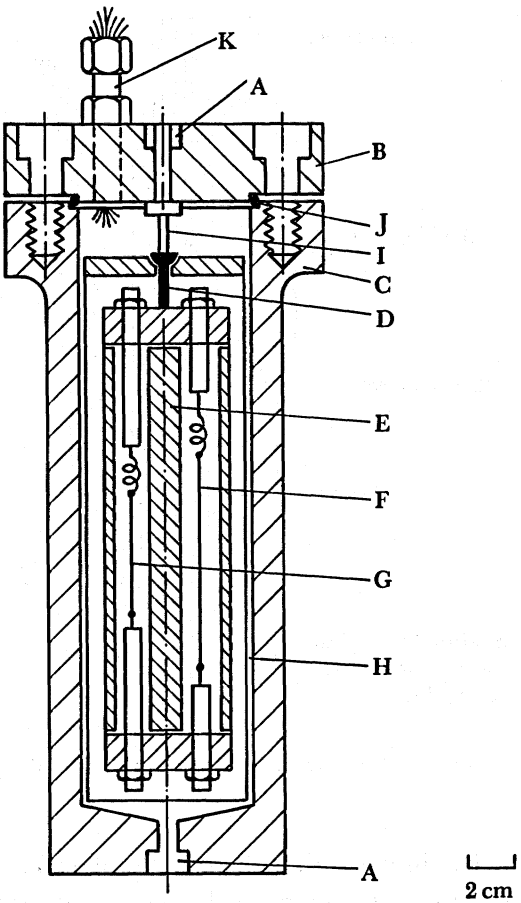

FIGURE 6. Section through the pressure vessel and cell.

when a heating voltage is applied. Secondly (and this is a problem particularly when extending the temperature range of the apparatus) they must accommodate the differential expansion between the cells and wires, which occurs when the temperature of the overall system is raised.

There is a considerable difference between the expansion coefficient of the wire (platinum: $9 \times 10^{-6}\ \mathrm{K}^{-1}$) and that of the cell body (stainless steel: $16 \times 10^{-6}\ \mathrm{K}^{-1}$). The new cells were therefore designed so that the wire ends were not attached to the walls, but were held apart by spacers which could be made of a suitable material, for example the ceramic 'Macor', which has an expansion coefficient of $9.4 \times 10^{-6}\ \mathrm{K}^{-1}$, similar to that of platinum.

Following the study by Haran & Wakeham (1982), beryllium–copper springs were first tried. Problems were experienced in joining these to the platinum wires and also corrosion problems were anticipated with the copper alloy and various polar gases like ammonia, which are intended for future study. Platinum–tungsten springs are therefore used and found successful in the temperature range up to 470 K. The alloy contained 8% tungsten and was used in the form of wire, 75 μm in diameter, supplied by the Sigmund Cohn Corp.

A simple helical spring is used to maintain the wire at approximately 25% of its ultimate tensile breaking load, which for 7 μm diameter wire is 4.7 mN. Springs with deflections per coil of less than half the coil radius and a pitch angle between the coils of less than 10° can be

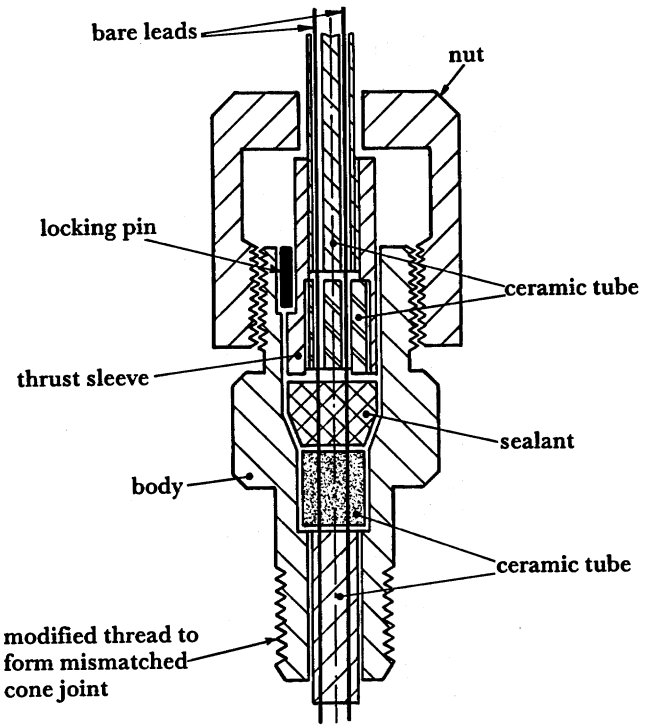

FIGURE 7. Electrical lead-through seals of the pressure vessel.

adequately designed by simple spring theory (Wahl 1963). By using these methods, springs were designed with three turns 5 mm in diameter and were found to give spring constants within 20% of their theoretical values. In both cells they were tensioned with a force of 1 mN, which gave an extension of about 2.3 mm. This tension was found to be adequate up to 470 K. The mass of the springs (about 25 mg) can be estimated to change the tension by about 10% as the cell is tilted from horizontal to vertical.

It is also necessary to take into account the fact that the use of a spring and/or weight to tension the wire gives rise to oscillation effects when the wire is heated rapidly during an experiment. These oscillations affect the bridge output because the wire resistances are affected by rapidly changing extension of the wire. These effects can be observed in our apparatus, but appear to be rapidly damped and do not seem to affect the results in a systematic way, as shown by the tests (e.g. the lack of variation in results with bridge voltage) given in §7.

It is also likely that the wires will creep under tension. This effect has been looked at with thicker wires in the same regions of stress over a wide range of temperature by Carreker (1950), who has shown that the amount of creep may not be negligible. The relation of creep against time for constant stress is an exponential decay, showing that most of the wire stretching occurs soon after applying the stress. The wire may stretch up to 1% of its original length under constant stress. This condition of constant stress is not met in a spring-tensioning system, and the amount of stretching of the wires after one day was not measurable. (This was in contrast to a previous system, in which a weight provided the constant stress. In that case the wires stretched gradually until after a few months measurements became impossible.) During cell assembly therefore, the wires were allowed to remain tensioned for several days before they

were mounted into the pressure vessel, and during this time a check was maintained on their lengths. Because of this effect and possibly others, it is also necessary to retension the wires after several months.

(*c*) *Geometry and method of connection*

Connecting the platinum filament to a platinum–alloy spring involves melting a sphere of gold of a standard size around both spring and the fine wire without melting the latter. This can be done with considerable precision by using a microtorch and a micromanipulator. First the spring is fused to a short length of 125 μm diameter gold wire by using the microtorch and micromanipulator combination. The gold wire is then cut close to the newly formed join leaving a stub of gold several millimetres long. A small sphere is then prepared on the end of the gold stub, by bringing the torch flame slowly up to the end of a wire, when it melts and forms a sphere. Its size can be controlled by adjusting the distance between the wires and the torch flame and the sphere is kept as small as possible.

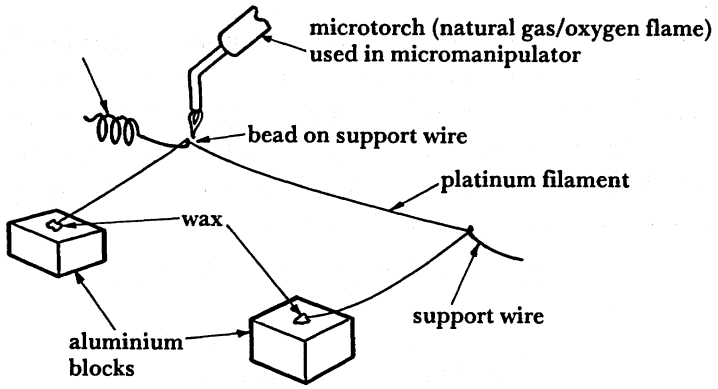

FIGURE 8. Wire mounting operation.

The wires are then mounted as shown schematically in figure 8. The fine platinum wire is lodged under the gold spheres at each end of the cells and maintained under a small tension by anchoring the ends to the metal blocks. The operation is done with a binocular microscope. The torch flame is then brought into proximity at one end; the sphere begins to melt and the fine platinum wire heats to a dull red, which aids viewing. The sphere increases in size as it absorbs more solid metal from the support wire, effectively moving down it. The platinum wire is 'sucked' into the sphere by surface tension and forms an electrical contact. The spare end of the fine platinum curve can now be melted away by using the torch. In this manner connections can be formed with repeatable geometries and without flux or any other contaminant present.

Once the connections have been made the supports are straightened and aligned with the cell axis as closely as possible. The wire is now annealed by passing an alternating current through the wire of sufficient strength to heat it to a dull red heat for about 2 min. This treatment removes any residual strains that are present in the wire, and also makes its resistance–temperature behaviour more stable. Finally, the wire is tensioned as described in the previous subsection, and the lengths of the wires, l_1 and l_2, are measured with a precision cathetometer.

(*d*) *Measurement of the wire temperatures*

The effect of using two wires in the configuration of figure 2 is that the measured temperature rise at any instant can be regarded as the temperature rise of a finite segment, length (l_1-l_2), of an ideal continuous line source. This will be true if the ends of the wires are very similar as shown in figure 1. The measured temperature rise, ΔT_m, of the 'effective wire' is given by

$$\Delta T_m = \{R_w(T)-R_w(T_0)\}/\{\alpha_0 R_w(T_0)\}, \tag{2.1}$$

where $R_w(T_0)$ is the resistance of the effective wire $(R_w = R_L-R_S)$ in the initial equilibrium state at the ambient temperature T_0. The term α_0 is the value for the temperature coefficient of resistance for the platinum wires in the region of T_0 to $T_0+\Delta T_m$ and is given by the equation

$$\alpha_0 = \{A+B(2T_0+\Delta T_m)\}/(1+AT_0+BT_0^2), \tag{2.2}$$

where

$$A = 3.98\times 10^{-3}\ \mathrm{K}^{-1}, \tag{2.3}$$

and

$$B = -10^{-4}\alpha\delta = -5.92\times 10^{-7}\ \mathrm{K}^{-2}. \tag{2.4}$$

The values quoted for the coefficients A and B were initially determined from calibration of the wire used in the hot-wire cells. However, the results of these experiments were, within experimental error, always equal to the values for pure annealed platinum published by Riddle *et al.* (1972) and so the latter values were always used. Because B is of the order of $10^{-7}\ \mathrm{K}^{-2}$ and ΔT_m is typically 7 K, α_0 can be considered constant over the temperature rise of the experiment with negligible error. Hence (2.1) becomes

$$\alpha_0(T_0) = (A+2BT_0)/(1+AT_0+BT_0^2). \tag{2.5}$$

3. Instrumentation

The electronic instrumentation for the apparatus will be dealt with here in general terms. The instrument package consists of a desk computer which controls the rig operations through two electronic equipment racks. Figure 9 shows a general view of the system layout. To the left of the computer is the thermal-conductivity bridge and its manual control/indicator panel housed in a small cabinet lined with polyurethane foam to stabilize the interior temperature. The thermal-conductivity bridge itself is protected from stray magnetic electric fields that would cause unwanted noise. The wires to the hot-wire cells are led from the front of the bridge unit and are insulated with polytetrafluoroethylene and are doubly screened. Further to the left is a rack containing the power supply, timers, pressure and temperature measurement and monitoring equipment.

Figure 10 shows a block diagram of the instrumentation. The desk-top computer, a Hewlett Packard HP9836S, is the main controller in the system. It gives information to the power supply and the bridge controller to initiate a measurement sequence. It also extracts the time intervals between successive bridge balances and the equilibrium temperature and pressure when a run has successfully terminated.

The bridge controller contains the logic that enables the automatic thermal-conductivity bridge to operate in any one of four modes, with an additional choice of eight resistor positions. It directs the timers to start and stop, following information from the bridge comparator that a null position has been reached. The bridge unit contains the thermal-conductivity bridge, of

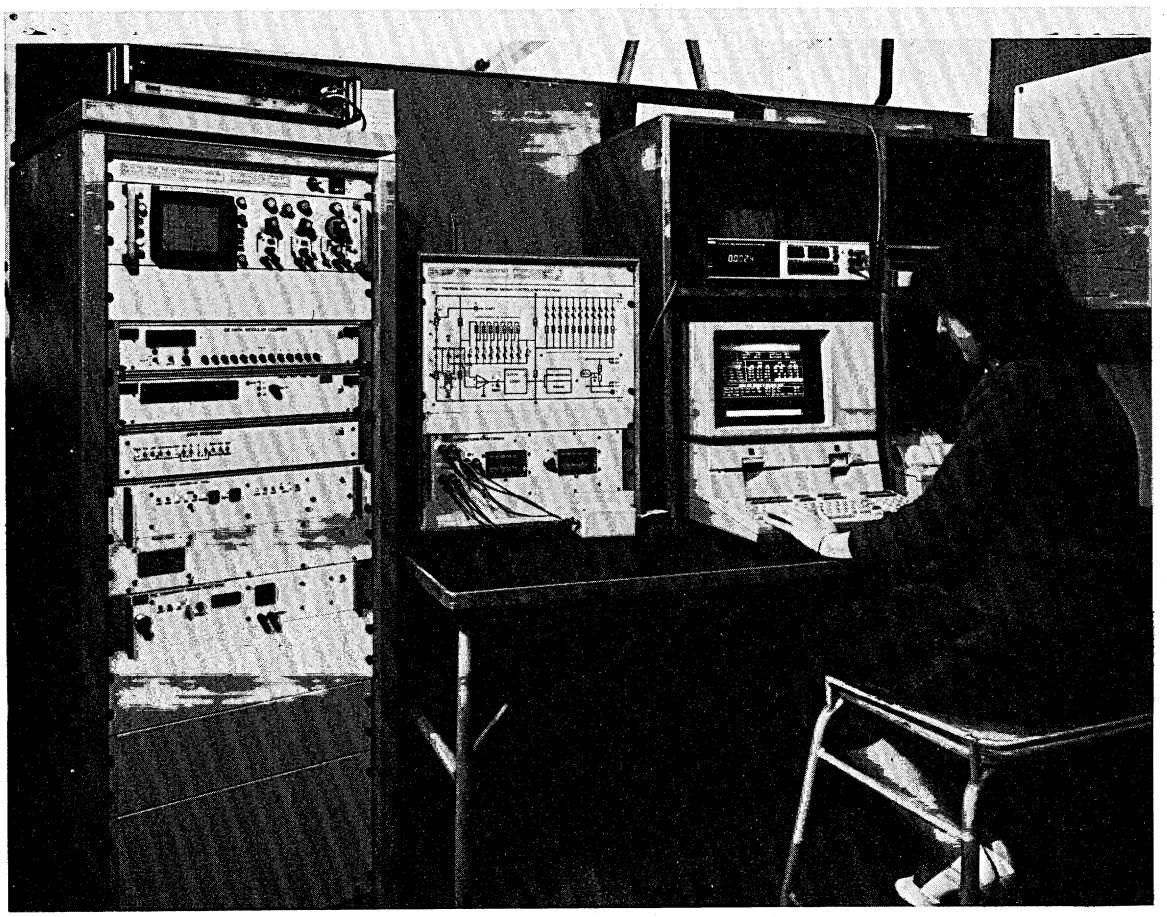

FIGURE 9. Instrument layout showing control computer and electronic equipment.

which the wires in the cells form part, and a comparator circuit, which detects the change in polarity across the bridge, as it passes through a balance point. The bridge is energized by a four-wire connection from the power supply directly on to the circuit board, thus eliminating unwanted voltage drops along cables. The comparator is carefully screened from magnetic and electric fields and is optically isolated from the subsequent logic circuits. In this way low noise levels are obtained, enabling the comparator to have a sensitivity of about 10 μV.

On a command from the computer keyboard, the bridge controller can be disabled and control is transferred to a manual controller. Manual control is used for certain operations such as measuring the wire resistances and for some exploratory experiments to determine optimum conditions. The bridge controller also displays the sequence of events during automatic operation.

(*a*) *Thermal conductivity bridge*

Figure 11 shows a schematic circuit of the automatic bridge that appears on the manual control panel. It is a Wheatstone bridge with arms XA′, A′X′, YF′, F′Y′. The thin platinum filaments are shown as R_L and R_S, the subscripts referring to long and short wires respectively, and are placed in series with the two variable resistance boxes R_1 and R_2 to form two arms of the bridge.

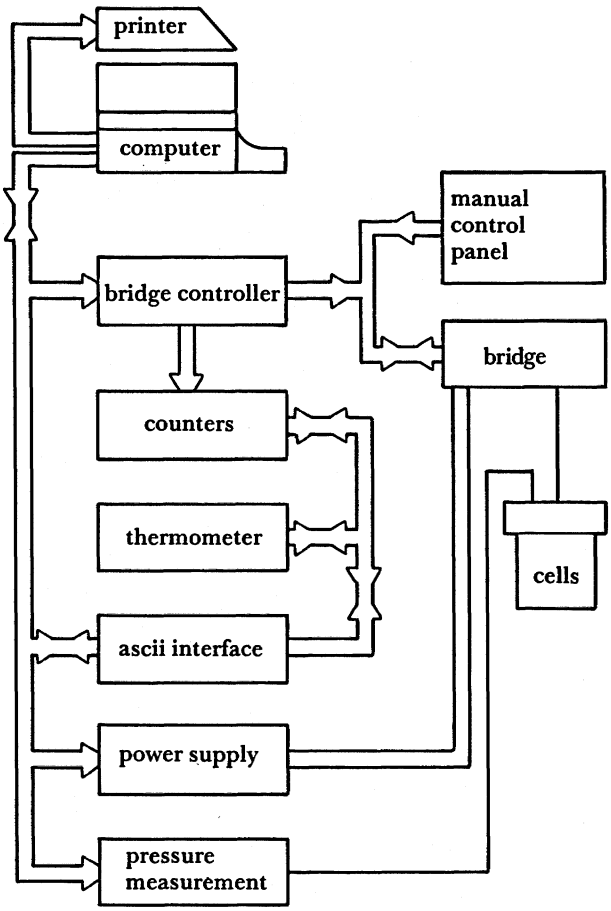

FIGURE 10. Block diagram of instrumentation arrangement.

The other two arms of the bridge are formed by a complex network of resistors to allow variation of experimental conditions. There are four 2 kΩ resistors and two banks of resistors R and S. The resistors in R are switched in or out rapidly during a single experiment to create a series of balance points. The configuration in the series S is selected before an experiment by closing one of the switches. The series S serves to modify the effect of the sequence of resistors in R. All resistors, including R_1 and R_2 are extremely high-precision high-stability types. Balance is detected by the sensitive comparator which produces a true (logic 1) signal, precisely as the bridge passes through balance. The state of balance monitored by light emitting diodes controls the switching logic to the timers and the R network as explained earlier. The manual switches are not actually in series with their corresponding resistors as shown in the diagram for clarity. The computer or manual switches operate reed relays, which perform the actual switching operations and turn the LEDs on and off.

We intend shortly to replace the series of resistances R and S, however, by a digital-to-analogue converter that will act to insert a program-controlled voltage into the bridge circuit (Wakeham 1986).

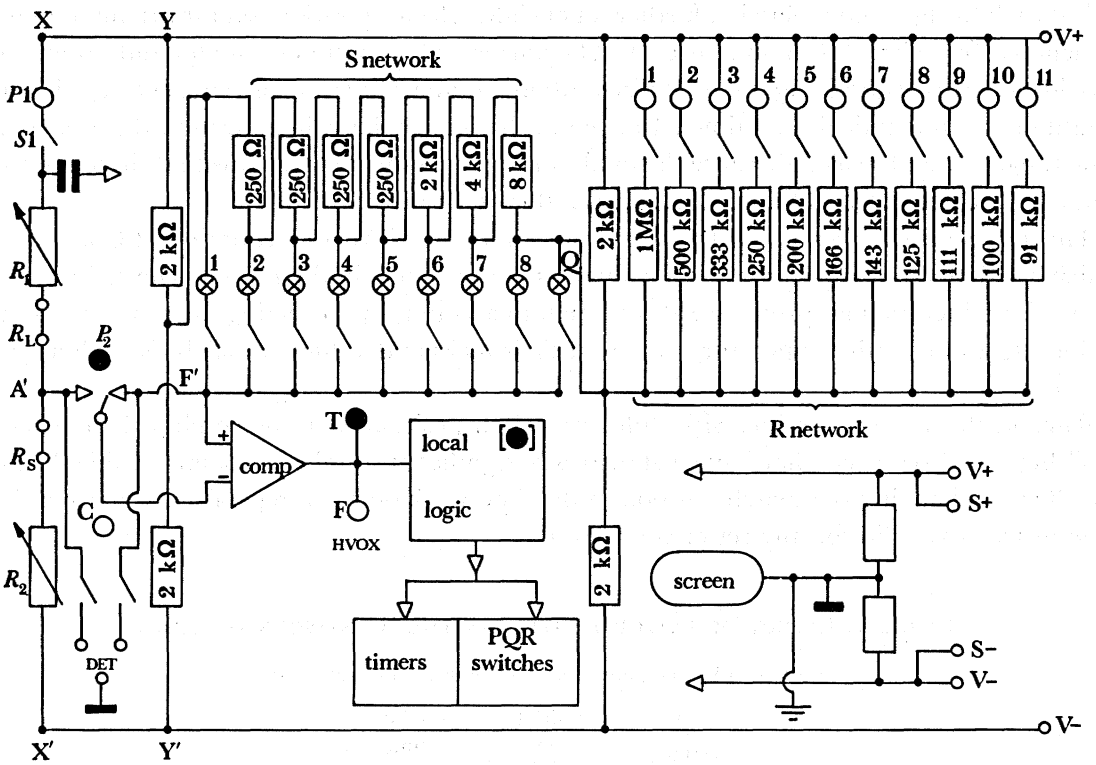

FIGURE 11. Manual control and indicator panel. Symbols: ○, red LED; ⊗, amber LED; ●, green LED.

(*b*) *Operation*

The R network can be switched in one of two ways, denoted sequential or substitution. In the sequential mode, at the start of a measurement, all the R resistors are in circuit and as the run progresses they are switched out one at a time, starting from switch 11, until all resistors are out of the circuit. The substitution mode operates as follows. Initially only switch 11 is in circuit. As the bridge goes through the first balance point switch 11 is opened and switch 10 closed. The substitution is repeated at successive balance points, each time a resistor of next higher value replacing its predecessor. At run termination all the R resistors are out of circuit.

A further two modes of operation are made possible by a switch Q, which when closed, effectively shorts out a portion of the attenuator chain S. The amount shorted out depends on the chosen switch positions in the S chain.

We can therefore define four distinct modes of operating the bridge, designated M1–M4. Each mode generates a reference 'voltage staircase' at the point F on the diagram of figure 11, between the reference arms of the bridge (as opposed to the measuring arms that contain the hot wires). Table 3 lists the various operating modes; the consequent flexibility enables a wide range of thermal conductivities to be measured.

TABLE 3. BRIDGE OPERATING MODES

mode no.	operating mode	switch Q
1	substitution	open
2	sequential	open
3	substitution	closed
4	sequential	closed

For each bridge mode there is a further set of eight selector positions on the attenuator chain S, denoted by switches 1–8 on figure 11. The various combination of modes and attenuators provide a means of obtaining different distributions of time points for a given set of experimental conditions with identical final times. In general the higher the switch position the greater the time range covered, which, because the final times remain the same, means that there are more points at shorter times as the higher numbered switches are closed.

The temperature rises are calculated from equation (2.5) and equations (3.25)–(3.27), which are derived below, and the known values of resistances in the bridge. The resistances of the leads and tensioning springs are also taken into account, by correcting the resistances of the springs, r_S, to the bath temperature, T_0, from their measured values at 293.15 K with a linear relation.

Runs in the same mode but with different switch positions may be combined to generate $\{\Delta T, \ln(t/\mathrm{ms})\}$ data sets that have a statistically significant number of points. Table 4 shows the effect of changing the switch position in the S network on the range of times covered. The general trend is valid for any set of conditions.

TABLE 4. EFFECT OF SWITCH POSITION IN THE S NETWORK ON TIMES

(Argon at 5.15 MPa and 38.87 °C; mode 1 measurement.)

switch position	initial time / ms	final time / ms
1	182	930
2	122	923
3	83	925
4	57	924
5	40	925

(c) *Bridge-balance equation*

Figure 12 shows a simplified version of figure 11 used to calculate the bridge-balance resistances. The resistor R_{ct} represents the equivalent parallel resistance in the R network in circuit at the balance point i, and R_a and R_b the resistances in the attenuator chain S for some arbitrary selector position. Using Kirchhoff's laws we can obtain five equations in the five unknown currents marked on figure 12.

With switch Q open we have

$$V = i_1(R_1 + R_2 + R_L + R_S), \tag{3.1}$$

$$V = i_2 R + i_3 R, \tag{3.2}$$

$$V = i_4 R + (i_2 - i_3 + i_4 + i_5) R, \tag{3.3}$$

$$i_2 R + (i_2 - i_3) R' = i_4 R, \tag{3.4}$$

and

$$i_4 R = i_5 R_{ct}. \tag{3.5}$$

Let

$$R_{ct}/R = a, \quad R_1 + R_2 + R_L + R_S = R_T, \tag{3.6}$$

$$R'/R = b, \quad \text{and} \quad R_T/R = y.$$

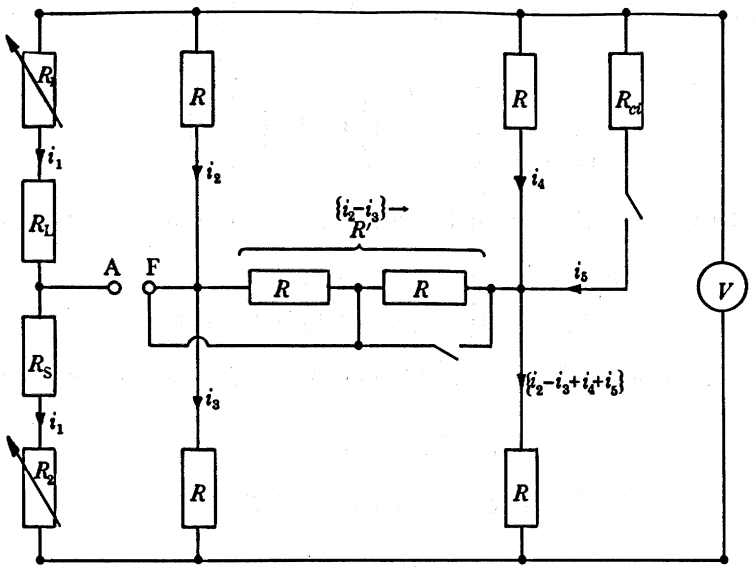

FIGURE 12. Bridge circuit for derivation of bridge balance equation.

Then
$$V/R = i_1 y, \tag{3.7}$$
$$V/R = i_2 + i_3, \tag{3.8}$$
$$V/R = 2i_4 + i_2 - i_3 + i_5, \tag{3.9}$$
$$i_2(1+b) - i_3 b = i_4, \tag{3.10}$$
and
$$i_4 = a i_5. \tag{3.11}$$

Substituting for i_4 in (3.9) and (3.10) we obtain
$$V/R = (2a+1)\, i_5 + i_2 - i_3, \tag{3.12}$$
and
$$i_2(1+b) - i_3 b - i_5 a = 0. \tag{3.13}$$

Also from figure 12 we can write for the potential across XF
$$V_{XF} = i_2 R + (i_2 - i_3) R_a, \tag{3.14}$$
or
$$V_{XF} = i_2 R + (i_2 - i_3)(R_a/R')\, R' = i_2 R + (i_2 - i_3)\beta R', \tag{3.15}$$
where $\beta = R_a/R'$. Therefore
$$V_{XF}/R = i_2(1+\beta b) - i_3 \beta b. \tag{3.16}$$
Now
$$V_{AF}/V = (V_{XA}/V) - (V_{XF}/V), \tag{3.17}$$
therefore
$$\frac{V_{AF}}{V} = \frac{R_1 + R_L}{R_T} - \frac{R i_2(1+\beta b)}{V} + \frac{i_3 \beta R}{V}. \tag{3.18}$$

We require to find expressions for i_2 and i_3 in terms of R and V. Equations (3.8), (3.12) and

(3.13) may be solved simultaneously for i_2, i_3 and i_5. Rewriting the equations in matrix form, we have

$$\begin{pmatrix} 1 & 1 & 0 \\ 1 & -1 & 2a+1 \\ 1+b & -b & -a \end{pmatrix} \begin{pmatrix} i_2 \\ i_3 \\ i_5 \end{pmatrix} = \begin{pmatrix} V/R \\ V/R \\ 0 \end{pmatrix}. \tag{3.19}$$

The solution to (3.19) when $V_{AF} = 0$ yields, after some manipulation, the result that

$$\frac{R_1+R_L}{R_T} = \frac{1}{2}\left[1 - \frac{(1+2\beta b)}{\{2(2a+1)(1+b)-1\}}\right]. \tag{3.20}$$

The above results were obtained for switch Q open. With Q closed the only change is to (3.4), which now becomes

$$i_2 R + (i_2 - i_3) R_a = i_4 R. \tag{3.21}$$

Thus
$$i_2 R + (i_2 - i_3) \beta R' = i_4 R, \tag{3.22}$$

and
$$i_2(1+\beta b) - i_3 \beta b = i_4, \tag{3.23}$$

where $b = R'/R$ as before. By using (3.23) in place of (3.10) and solving as before leads directly to

$$\frac{R_1+R_L}{R_T} = \frac{1}{2}\left[1 - \frac{(1+2\beta b)}{\{2(2a+1)(1+\beta b)-1\}}\right]. \tag{3.24}$$

Thus all that has changed in the final result is that the parameter b in the denominator of (3.20) is now multiplied by the factor β.

The preceding derivations express the sum of the long and short wire resistances in terms of known resistances. What we require to measure experimentally is the difference in resistance between the long and short wires R_w. Both (3.20) and (3.24) can be put into the form

$$R_w = (R_L - R_S) = \frac{(C_t R_2 - R_1)(R_L/R_S - 1)}{\{(R_L/R_S) - C_t\}}, \tag{3.25}$$

where
$$C_t = \frac{(2a+1)(1+\delta b) - (\beta b + 1)}{(2a+1)(1+\delta b) + \beta b}, \tag{3.26}$$

and
$$\delta = 1, \text{ if Q is open}; \quad \delta = \beta, \text{ if Q is closed.} \tag{3.27}$$

The ratio R_L/R_S in (3.25) can be equated to the ratio of the long and short wire resistances at the bath equilibrium temperature as the temperature rises of the wires are approximately the same. The error introduced in doing this is negligible, because the temperature rise of the wires is small. For a given run δ, β and b are constants but a changes at each balance point because of the change in the R network.

(*d*) *Time measurement*

During a run the control logic of the bridge controller starts and stops the set of 12 timers, in such a way that each timer records the time interval between two successive bridge balances, except the first, which records the interval between energizing the bridge and the first balance. The process of stopping one timer and starting the next is done with negligible delay. Each timer is clocked from the same reference oscillator and can resolve intervals to 10 μs. The

maximum interval possible is 999.99 ms and the shortest approximately 4 ms. The lower limit was introduced to prevent spurious triggering of the comparator.

Errors in the measurement of the time intervals arise directly from the noise levels present across the bridge and at the comparator input. For convenience it is useful to consider a single bridge balance where a noisy bridge signal passes through zero and triggers a noiseless comparator, as shown in figure 13 where the true time of balance is marked at the point 0.

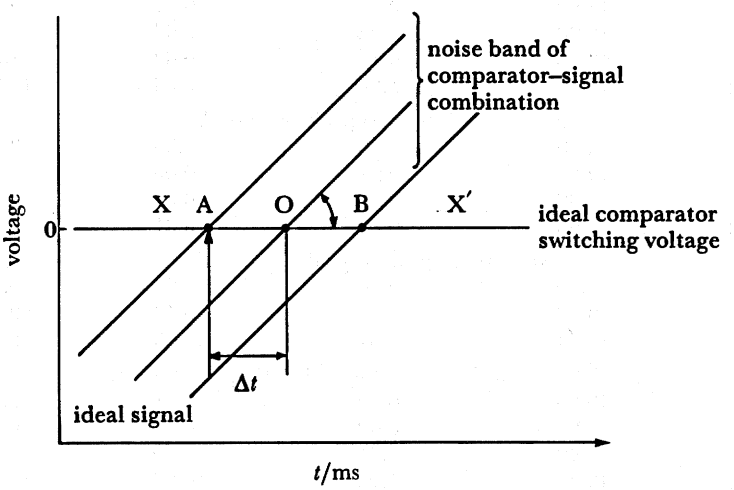

FIGURE 13. Time errors due to noise on bridge signal.

Because the comparator switches the instant signal voltage crosses zero, the detected switching time will be shifted systematically to the left if the frequency of the noise signal is high (in the worst case to the point A). The amount of shift or bias depends on the rate of the voltage rise across the bridge, and is greater at longer times where the time intervals between balances are longer. Examining a worst case, we have from figure 2

$$\Delta t_{\max} = V_N/2(\mathrm{d}V/\mathrm{d}t). \tag{3.28}$$

V_N can be regarded as an effective peak-to-peak noise signal for the bridge–comparator combination, and is given by

$$V_N^2 = V_c^2 + V_s^2, \tag{3.29}$$

where V_c is the comparator peak-to-peak input noise, and V_s is the peak-to-peak signal noise.

In the apparatus the signal to the comparator is bandwidth limited to 10 kHz, which implies that the maximum frequency component in the noise band has a period of 100 μs. A computer simulation of this problem was carried out in which a random noise voltage was superimposed on to a linear ramp of known period. The mean time taken for the ramp to reach a standard voltage was compared to the ideal time for a noiseless signal, for 20 crossover events. Table 5 details the results obtained and shows that a systematic left bias of the time interval occurs which increases with decreasing signal slope as predicted. Also the mean bias was, in the worst cases, approximately two thirds of the maximum possible bias calculated from (3.28) and (3.29) and given in the last column.

The experimentally determined noise level of the bridge–comparator system was found to be

TABLE 5. RESULTS OF THE COMPUTER SIMULATION OF A CROSS-OVER EVENT IN THE COMPARATOR WITH A NOISY SIGNAL

(True period = 50.00 ms in all cases. Each point is an average of 20 events.)

slope / V s^{-1}	mean period / ms	standard deviation / ±ms	time bias / ms	maximum bias / ms
	$v_s = \pm 10$ μV peak-to-peak: $v_c = 0$ μV			
1.0	49.99	0.00	0.01	0.01
0.1	49.93	0.02	0.07	1.1
0.01	49.38	0.17	0.62	1.0
0.001	43.33	1.86	6.68	10.0
	$v_s = \pm 5$ μV peak-to-peak: $v_c = 0$ μV			
1.0	50.00	0.00	0.00	0.005
0.1	49.97	0.01	0.03	0.05
0.01	49.68	0.08	0.32	0.50
0.001	46.69	0.83	3.31	5.0
	$v_s = \pm 20$ μV peak-to-peak: $v_c = 0$ μV			
1.0	49.99	0.00	0.01	0.02
0.1	49.87	0.04	0.13	0.20
0.01	48.74	0.31	1.26	2.0
	$v_s = \pm 10$ μV peak-to-peak: $v_c = \pm 2$ μV peak-to-peak			
1.0	49.99	0.00	0.01	0.01
0.1	49.93	0.02	0.07	0.1
0.01	49.42	0.21	0.59	1.0
0.001	43.34	1.72	6.66	10.0

about 10 μV peak-to-peak with a thermal electromotive force offset at points A and F (see figure 12) of between 50 and 100 μV. The offset however could be compensated for by adjusting the comparator by using the comparator trim control situated on the front panel of the thermal-conductivity bridge. With these noise levels and from the results of the computer simulation, a time-bias correction was applied to the experimental times. The voltage rise between successive bridge balances (comparator cross-overs) was assumed to be linear for this purpose. By calculating the voltage change immediately after a balance condition when the resistance of the hot wires are taken to be the same as at balance, the slope of the voltage rise can easily be computed for all except the first time points. The first time point is left unaltered because the slope of the voltage rise across AF is sufficiently great to make the bias negligible. The maximum time bias is calculated from (3.28) and (3.29) and multiplied by the factor 0.667 in accordance with the simulation results, which showed that the most likely bias was about two thirds of the maximum. The magnitude of this correction is only just significant for the most precise work, being of the order of 0.1–0.2 %.

4. TEMPERATURE AND PRESSURE MEASUREMENT AND CONTROL

(*a*) *Temperature measurement*

The equilibrium temperature of the hot-wire cells, determined by using a platinum resistance element that conforms to BS 1904, Grade 1, is inserted into a well in the pressure vessel cap. The element was further calibrated *in situ* against a primary transfer standard thermometer to obtain its resistance at 0 and 100 °C and hence its temperature coefficient of resistance, α. The element can measure temperatures in the range 0–100 °C with an accuracy of 0.01 K. However,

an additional error is introduced when the thermometer is coupled to an electronic unit that displays the temperature directly in degrees Celsius. The electronic unit has two adjustable parameters. The first adjusts the base-line temperature and the second the slope of the temperature–resistance relation. It is the setting of these parameters that determines the overall accuracy of the temperature measurement system. The thermometer system has an overall accuracy of better than 0.05 K, which is adequate.

(*b*) *Temperature control*

Figure 14 shows a schematic section through the air bath. It consists of a set of four concentric cylindrical shells A, B, C and D, connected to form a closed system of canals. Air is circulated continuously around the system by a fan (F) mounted at the base of the unit and driven by a

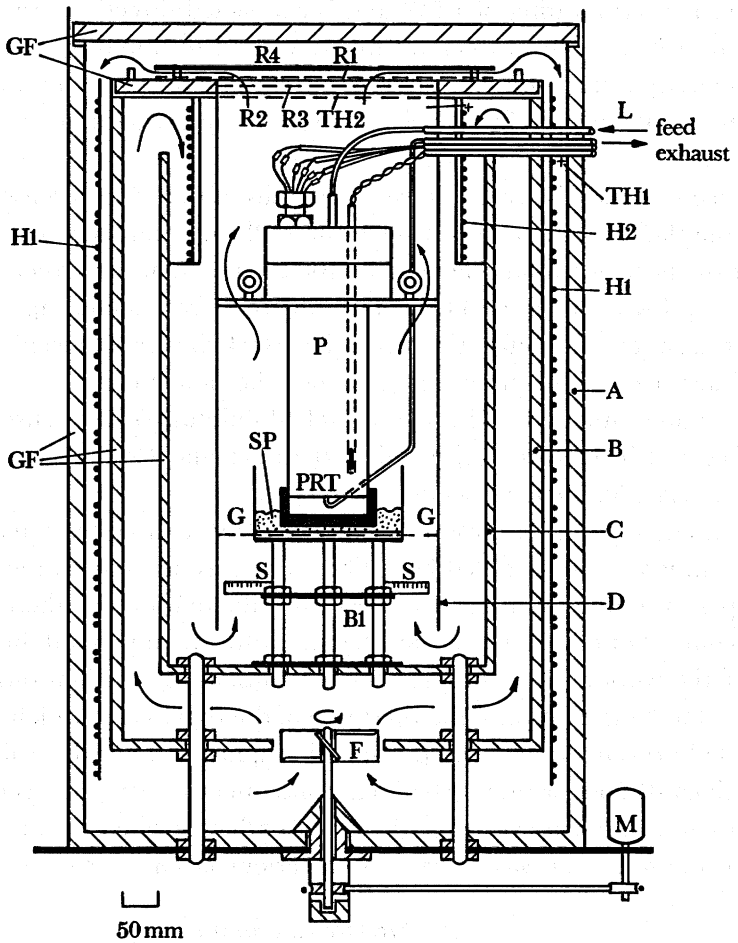

FIGURE 14. Schematic section through the air-bath thermostat.

motor (M). Air is drawn past a backing heater element (H1) in the annulus formed by A and B; through a cavity between B and C; past a control heater (H2) mounted in the annulus between C and D; over the control sensor (S); and past the pressure vessel (P). Once above P the air passes through four radiation screens (R1 to R4) before being drawn down once again between A and B to begin another circuit. A, B and C consists of a sandwich of glass-wool

insulation between metal sheets: D has no insulation and provides an isothermal surface at the same temperature as P. The four auxiliary radiation screens placed above P improve the axial temperature uniformity of the central area of the thermostat. Initially only three expanded metal mesh screens (R1 to R3) were used but only with the addition of the solid stainless-steel polished shield (R4) did the axial temperature gradients become insignificant. The pressure vessel stands in a metal pot (SP) full of pond sand to provide some vibration damping. This pot rests on a small metal stool that supports the pressure vessel and carries the control sensor for H2. The sensor is protected from damage by a stainless steel gauze disc (G).

Electrical connections and gas supply and exhaust lines to the pressure vessel are made by way of five 25 mm outside-diameter thin-walled stainless-steel tubes (L) which are inserted through the thermostat walls about 50 mm above the top of P. Both heating elements (H1 and H2) are of the mineral-oxide insulated stainless-steel sheathed type. H1 has a maximum power rating of 6 kW. H2 has a rating of 1 kW and is connected directly to the thyristor unit of the temperature controller. Both heaters are bifilar wound to minimize induction effects on the thermal conductivity cells mounted in the thermostat. Four sensors are installed in the central area of the thermostat: two platinum resistance sensors and two thermocouple junctions, which are described below.

(*a*) Resistance sensors. Figure 15 shows the details of the control sensor (S) mounted on to plate (B1) of the thermostat. It consists of 1.4 m of 25 μm diameter platinum wire wound on to six mica formers to make an element of 100 Ω (nominal resistance at 0 °C). The other resistance sensor, PRT in figure 14, is a commercial ceramic-encapsulated device, whose temperature resistance characteristic meets BS 1604 Grade 1 specification and that was calibrated against a standard platinum resistance thermometer.

(*b*) Thermocouple junctions. The two nickel–aluminium/nickel–chromium thermocouple junctions (TH1 and TH2) are positioned next to H1 and H2 respectively, and are used as safety cut-out sensors for their respective heaters.

The temperature of the thermostat is controlled by a three-term temperature controller enclosed in a temperature-controlled box. The latter was needed to prevent long-term drift of the bath temperature due to ambient temperature fluctuations on the controller set point.

The final control obtained in the air temperature at any point in the thermostat was ±0.03 K over the working day. Because the air temperature oscillations are relatively fast it is unlikely that the temperature of the thermal-conductivity cells, which are contained within the heavy-walled pressure vessel, would respond as quickly. Thus the cell-temperature control should be significantly better than ±0.03 K. Subsequent measurements on the stability of the wire resistances in the pressure vessel inside the air bath confirmed this and temperature control of ±15 mK in the test fluid was realized over periods of an hour or so.

(*c*) *Pressure measurement*

Figure 16 shows a schematic diagram of the complete pressure circuit. Gas from the storage bottle A is passed through a particle filter into an air-operated diaphragm compressor, DC. The outlet pressure from the compressor can be regulated by adjusting the air supply to it through valve V2, monitored by gauge G3. If pressures less than about 10 MPa are required, gas passes directly through the compressor without compression. Two dial gauges, G1 and G2, monitor the inlet and outlet pressures of the compressor.

The gas is fed via a high-pressure chromatography valve, HPV, and a high-pressure–high-temperature valve V9, to the pressure vessel, P. V10 and V11 (similar to V9) allow the vessel

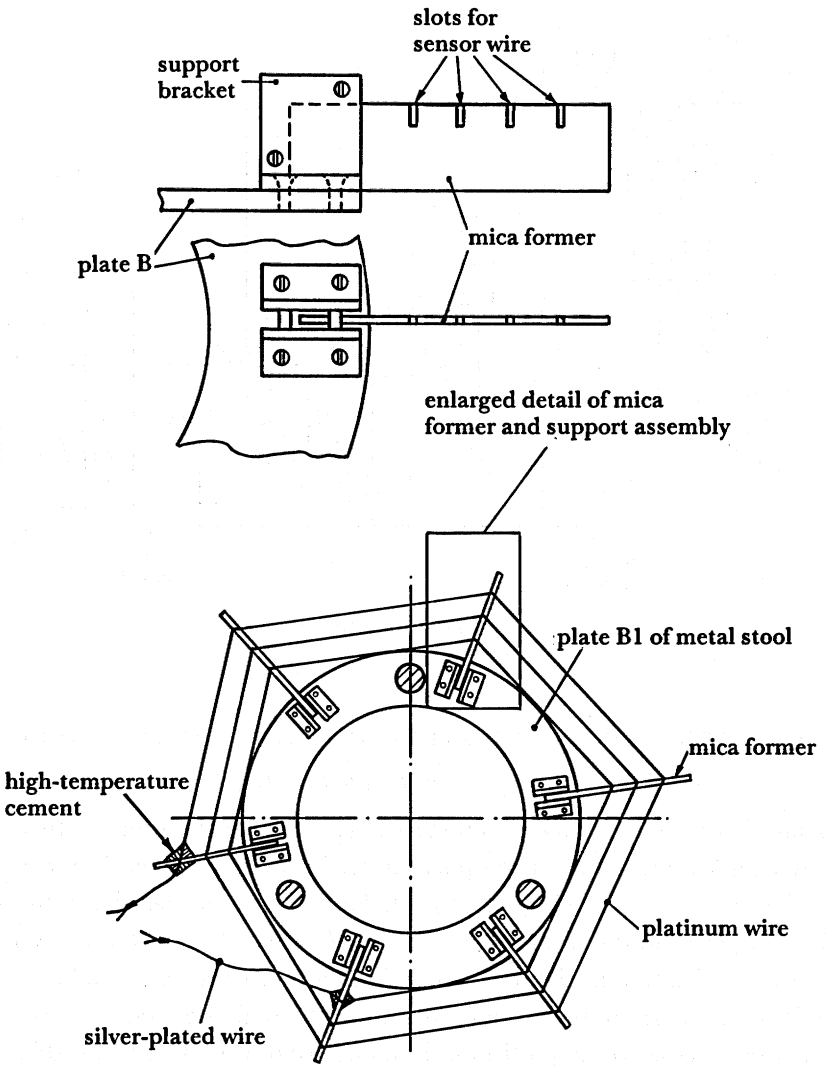

FIGURE 15. Detail of control sensor mounting.

to be exhausted or fed to a sample vessel. There is also a high-pressure system that can feed liquids via HPV into P. It consists of a liquid reservoir, L, an accurately calibrated syringe, R, and a pressure gauge, G4. Pressure is maintained with a SETRA 204 capacitance pressure transducer, PT, and a digital voltmeter.

Calibration of the transducer was carried out using a Budenburg model 280D deadweight tester. The piston of this tester had been calibrated against a primary standard traceable to the National Physical Laboratory. The tester is capable of measuring pressures with an accuracy of $\pm 0.3\,\%$ at 20 °C $\pm$ 1 °C. The transducer exhibits a linear response in voltage (in the range 0–5 V) as a function of the applied gas pressure, is filled with mercury to eliminate dead volume and is thermostatically controlled at 30 °C $\pm$ 0.5 °C to further stabilize the voltage output with respect to changes in ambient temperature. With this arrangement pressure can be measured with an uncertainty of 0.1 % in the range 10–300 bar.†

† 1 bar = 10^5 Pa.

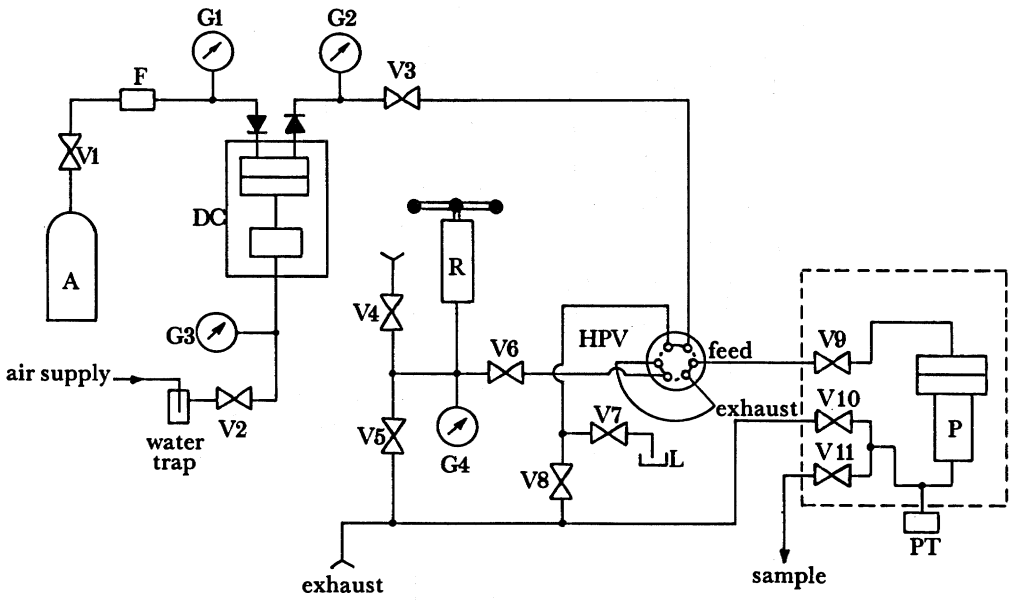

FIGURE 16. High-pressure system.

5. CORRECTIONS AND LIMITATIONS TO THE IDEAL MODEL

(*a*) *End effects and finite wire length*

There is no simple analytical way to obtain a correction to the temperature rise of a finite platinum wire with fixed ends. Two attempts at describing the problem in recent literature are by Healy *et al.* (1976) and by Haarman (1971). Haarman considered the finite wire in two ways: (*a*) a 'floating wire' in the fluid medium; and (*b*) a wire connected to two infinite planes normal to the wire axis and maintained at a constant temperature. He concluded that the effect of boundary (*b*) is twice as great as that of (*a*) and that the real effect lies somewhere in between the two. If the support wires to the platinum filament are not too thick, the effect will be closer to case (*a*) of a floating wire. In both cases he neglected the axial heat flow through the wire to its supports, i.e. axial conduction for $r \leqslant a$.

Healy *et al.* (1976) followed an earlier analysis given by Blackwell (1956) who considered the temperature field in an infinite fluid bounded internally by a cylinder of radius a. Neglecting the non-uniform temperature distribution within the wire (i.e. $r \leqslant a$) he assumed that the heat flux only exists over some arbitrary length L of the wire. Solution of the resulting differential equation gave an expression for an upper limit δ to the fractional error in the measured thermal conductivity, which included the effect of axial conduction along the wire.

$$\delta = \frac{\exp(-L^2/16\tau)}{\sqrt{\pi}} \left\{ \frac{\sqrt{(16\tau)}}{L} + \frac{L}{a} \left(\frac{\lambda_w}{\lambda_f} - \frac{\rho_w c_{p,w}}{\rho_f c_{p,f}} \right) \frac{\ln(4\tau/a^2 C)}{(4\tau/a^2)^{\frac{3}{2}}} \right\}, \tag{5.1}$$

where

$$\tau = \kappa_f t. \tag{5.2}$$

The first term within the large parentheses on the right-hand side of (5.1) relates to axial conduction through the medium and the second term, axial conduction through the wire. For all cases of concern the conduction through the wire may be neglected. A feasibility study by Wakeham has shown that, for a limit of $\delta = 0.0001$ and a wire radius of 7 μm, a minimum

length of wire equal to 70 mm is required. The only criterion being that measurements are restricted to fluids with thermal diffusivity less than 5×10^{-5} m^2 s^{-1}, which in practice means an experimental low-pressure limit of between 0.5–1.0 MPa.

However, the preceding analyses are still only approximate and do not include the effects of convection at the ends. Most experimental apparatus use design techniques to reduce end effects to acceptable levels. There are two possible ways of doing this: either use potential taps (Briggs 1965; Roder 1981) across the central portion of the wire or use two wires (de Groot *et al.* 1978) of different lengths in adjacent arms of an electrical bridge circuit. The latter possibility was adopted in the design of our apparatus for several reasons. Firstly the practical problems of attaching a potential tapping to a 7 μm diameter wire would be severe. Secondly, any potential tap would provide an alternative high thermal-conductivity path for the heat flux generated by the line source, and the axial temperature profile of the line source at any instant would exhibit dips at the point of attachment of the potential tappings.

Unfortunately, using two wires to eliminate end effects introduces a problem of non-uniformity. Because in general, even if the wires come from the same spool, they will have different average radii, so they will also have different heat dissipations and temperature rises, which means that the simplified picture above will not be exact. Moreover, the end effects will not precisely cancel, but this is only of second order as these effects are weak functions of the wire radii, and need only be considered if the wires are grossly different. Kestin & Wakeham (1978) have recently considered the problem of non-uniformity of the wires and the following analysis is based on theirs. The differences in the dimensions of the two wires can be characterized by their resistance per unit length σ, with subscript 1 referring to the long wire and 2 to the short wire. Thus we can define a quantity ϵ, which is zero for identical wires, by

$$\epsilon = 1 - (\sigma_2/\sigma_1), \tag{5.3}$$

where

$$\sigma_1 = R_1/l_1, \tag{5.4}$$

and

$$\sigma_2 = R_2/l_2. \tag{5.5}$$

For the wires used in our apparatus $|\epsilon| \leqslant 0.02$.

Equation (2.1) describes the measured temperature rise of the 'effective' wire. Individually, however, the long and short wires will have individual temperature rises and resistance changes related as follows:

$$\Delta T_1 = \{R_L(T) - R_L(T_0)\}/\{\alpha_0 R_L(T_0)\}, \tag{5.6}$$

and

$$\Delta T_2 = \{R_S(T) - R_S(T_0)\}/\{\alpha_0 R_S(T_0)\}. \tag{5.7}$$

In (5.6) and (5.7) the possibility of different end effects in the two wires has been neglected, as it is a second-order correction. The temperature rise actually measured, ΔT_m, can be related to ΔT_1 and ΔT_2 and is given by

$$R_w(T_0)\,\Delta T_m = R_L(T_0)\,\Delta T_1 - R_S(T_0)\,\Delta T_2. \tag{5.8}$$

The temperature rises of the fluids adjacent to each wire will be given ideally by equations of the form of (1.8).

$$\Delta T^{(1)}_{id}(a_1, t) = (q_1/4\pi\lambda_f) \ln (4\tau/a_1^2 C), \tag{5.9}$$

and

$$\Delta T^{(2)}_{id}(a_2, t) = (q_2/4\pi\lambda_f) \ln (4\tau/a_2^2 C), \tag{5.10}$$

where superscripts (1) and (2) refer to ideal long and short wires respectively.

The actual temperature rises will be different in practice but we now assume that the ratio of the infinite line source temperature rises $\Delta T_{id}^{(1)}/\Delta T_{id}^{(2)}$ equals the ratio of the actual temperature rises, which is a good approximation because all corrections to the ideal case are less than 0.5%. Thus,

$$\Delta T_1/\Delta T_2 = \Delta T_{id}^{(1)}/\Delta T_{id}^{(2)}, \tag{5.11}$$

which can be substituted into (5.8) to give

$$R_w(T_0)\,\Delta T_m = R_L(T_0)\,\Delta T_1 - R_S(T_0)\,\Delta T_1(\Delta T_{id}^{(2)}/\Delta T_{id}^{(1)}) \tag{5.12}$$

and

$$R_w(T_0)\,\Delta T_m = \Delta T_1\{R_L(T_0) - R_S(T_0)\,(\Delta T_{id}^{(2)}/\Delta T_{id}^{(1)})\}. \tag{5.13}$$

From (5.9) and (5.10) we have

$$\frac{\Delta T_{id}^{(2)}}{\Delta T_{id}^{(1)}} = \left(\frac{q_2}{q_1}\right)\frac{\ln(4\tau/a_2^2 C)}{\ln(4\tau/a_1^2 C)}. \tag{5.14}$$

The ratios (q_2/q_1) and (a_1^2/a_2^2) are related to the ratios of resistances per unit length σ_1 and σ_2 and the quantity ϵ (see (5.3)–(5.5)) by

$$q_2/q_1 = i^2\sigma_2/i^2\sigma_1 = 1-\epsilon, \tag{5.15}$$

and also

$$a_1^2/a_2^2 = \sigma_2/\sigma_1 = 1-\epsilon. \tag{5.16}$$

Substituting for a_1^2 and q_2/q_1 in (5.14) results in

$$\frac{\Delta T_{id}^{(2)}}{\Delta T_{id}^{(1)}} = \frac{\{(1-\epsilon)\ln(4\tau/a_2^2 C)\}}{\{\ln(4\tau/a_2^2 C) - \ln(1-\epsilon)\}}. \tag{5.17}$$

Now for $|\epsilon| \ll 1$,

$$\ln(1-\epsilon) = -\epsilon, \tag{5.18}$$

and therefore

$$\frac{\Delta T_{id}^{(2)}}{\Delta T_{id}^{(1)}} = \frac{(1-\epsilon)}{\{1+\epsilon/\ln(4\tau/a_2^2 C)\}}, \tag{5.19}$$

$$\approx 1-\epsilon', \tag{5.20}$$

to first order in the parameter ϵ, where

$$\epsilon' = \epsilon\left\{1+\frac{1}{\ln(4\tau/a_2^2 C)}\right\}. \tag{5.21}$$

Finally substitution for the ratio $\Delta T_{id}^{(2)}/\Delta T_{id}^{(1)}$ in (5.13) yields the result

$$R_w(T_0)\,\Delta T_m = \Delta T_1\{R_L(T_0) - R_S(T_0)\,(1-\epsilon')\}, \tag{5.22}$$

or

$$\Delta T_1 = \Delta T_m/C_1(t), \tag{5.23}$$

where

$$C_1(t) = 1 + [R_S(T_0)/R_w(T_0)]\,\epsilon'. \tag{5.24}$$

Equation (5.23) gives the temperature rise of the long wire acting as a finite segment of an infinite wire in terms of the measured temperature rise ΔT_m, the nominal wire radius a_2, the initial equilibrium values of the wire resistances and a first estimate of the fluid diffusivity.

PHILOSOPHICAL TRANSACTIONS OF THE ROYAL SOCIETY A MATHEMATICAL, PHYSICAL & ENGINEERING SCIENCES

(*b*) *Finite radius of the line source*

The effect of replacing the ideal line source with one of radius $r = a$ can be found by solving the Fourier equation (1.1) subject to the new boundary condition for $r = a$ and all $t \geqslant 0$.

$$\partial T/\partial r = -q/2\pi\lambda_f a. \tag{5.25}$$

Once again for values of $r^2/4\kappa_f t \ll 1$ the solution reduces to

$$\Delta T(r,t) = (q/4\pi\lambda_f) \ln (4\kappa_f t/r^2 C) + O(a^2/\kappa_f t). \tag{5.26}$$

In a typical experiment the term $a^2/\kappa_f t$ has a value of less than 10^{-8}. The first term of (5.26) is the basic solution given in (1.8). Thus the temperature rise of the fluid surrounding the line source is hardly dependent on the radius of the line source and hence exact cylindricity is not important for a practical line source.

(*c*) *Finite thermal conductivity and heat capacity of the wire*

Equation (1.8) and subsequent equations give the temperature rise of the fluid. The temperature of the wires will be equal to that of the adjacent fluid only if their thermal conductivity is infinite and their heat capacity is zero. To account for the finite heat capacity and thermal conductivity of the wire, the mathematical problem is changed from the ideal continuous line source to one involving a composite cylinder. The cylinder is imagined to consist of an inner region $0 \leqslant r \leqslant a$, which is the wire, and an outer region $a < r < \infty$, which is still regarded as an infinite incompressible fluid of diffusivity κ_f. Two additional constraints are also applied: that the temperature and heat flux must be continuous between the two regions at $r = a$. Thus we have two coupled Fourier equations to solve, one for the wire and one for the fluid. Because we have constrained the temperature of the two regions to be the same at $r = a$, we need only concern ourselves with the wire temperature at $r = a$ (because this is what we measure indirectly in practice). The problem can be further simplified by considering the cases (*a*) when wire has infinite thermal conductivity and finite heat capacity, and (*b*) when the wire has finite thermal conductivity and finite heat capacity. These problems are discussed by Carslaw & Jaeger (1959, pp. 345, 347). The solutions for the wire temperature rise at $r = a$ are as follows.

Case (*a*): $C_{p,w}$ = finite, $\lambda_w = \infty$,

$$\Delta T_w(a,t) = \frac{2q\omega^2}{\pi^3\lambda_f} \int_{u=0}^{u=\infty} \frac{\{1-\exp(-\kappa_f t u^2/a^2)\}\,du}{u^3[\{uJ_0(u)-\omega J_1(u)\}^2+\{uY_0(u)-\omega Y_1(u)\}^2]}, \tag{5.27}$$

Case (*b*): $C_{p,w}$ = finite, λ_w = finite,

$$\Delta T_w(a,t) = \frac{4q}{\pi^3\lambda_f L^2} \int_{u=0}^{u=\infty} \frac{\{1-\exp(-\kappa_w t u^2/a^2)\}\,J_0(u)\,J_1(u)\,du}{u^4\{A^2(u)+B^2(u)\}}, \tag{5.28}$$

where
$$A(u) = \lambda_w \kappa_f^{\frac{1}{2}}\{J_1(u)\,Y_0(Ku) - (K/L)\,J_0(u)\,Y_1(Ku)\}, \tag{5.29}$$

and
$$B(u) = \lambda_w \kappa_f^{\frac{1}{2}}\{J_1(u)\,J_0(Ku) - (K/L)\,J_0(u)\,J_1(Ku)\}. \tag{5.30}$$

Also
$$K = \sqrt{(\kappa_w/\kappa_f)}, \tag{5.31}$$

$$L = \lambda_w/\lambda_f, \tag{5.32}$$

and
$$\omega = 2\rho_f c_{p,f}/\rho_w c_{p,w}. \tag{5.33}$$

$J_\nu(u)$ is the Bessel function of the first kind of order ν and $Y_\nu(u)$ is the Bessel function of the second kind of order ν.

It is more convenient for calculation purposes to work in dimensionless reduced temperature rises θ_i^* defined by

$$\theta_i^* = \{\Delta T_w(a,t)\}_i/(q/4\pi\lambda_t). \tag{5.34}$$

Applying this to (1.8), (5.27) and (5.28) we obtain for the ideal case:

$$\theta_0^* = \ln(\kappa_t t/a^2), \tag{5.35}$$

for case (a):
$$\theta_1^* = (8\omega^2/\pi^2)\int_0^\infty Q1\,\mathrm{d}u, \tag{5.36}$$

and for case (b):
$$\theta_2^* = (16/\pi^2 L^2)\int_0^\infty Q2\,\mathrm{d}u, \tag{5.37}$$

where $Q1$ and $Q2$ are the integrands given in (5.27) and (5.28) respectively.

Complete analytic solutions to (5.36) and (5.37) are not possible and so the integrations were performed numerically. A large number of results were obtained for a variety of typical κ_t and ω values. These are conveniently summarized in figures 17 and 18, which show the following.

(a) $\theta_1^* = \theta_2^*$ to within three decimal places for all values of ω at all but the smallest times (less than 0.1 ms), which can be neglected for our purposes. Thus for typical experimental parameters the effect of finite thermal conductivity of the wire is negligible.

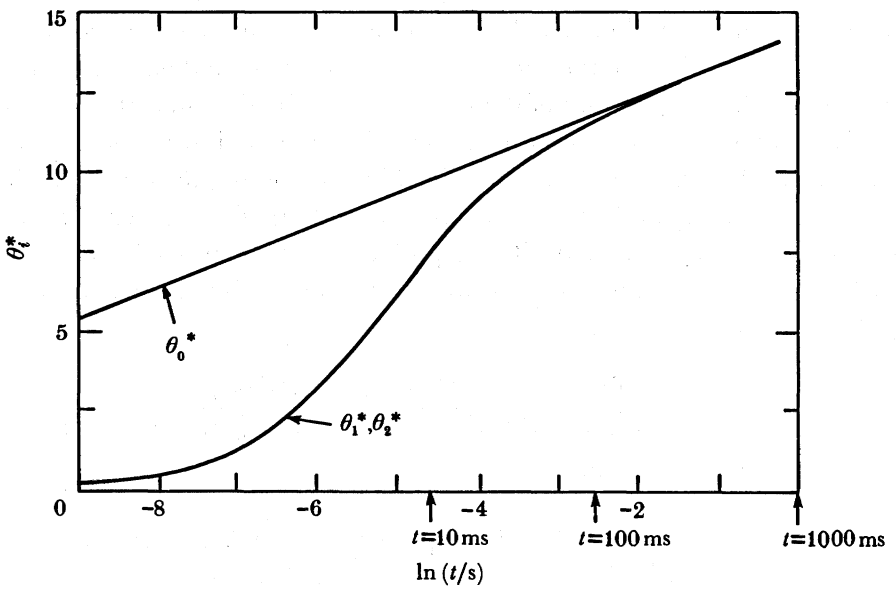

FIGURE 17. Comparison of θ_1^* and θ_2^* with θ_0^* for small ω; $\lambda_t = 0.0145$ W m^{-1} K^{-1}, $\omega = 0.001$.

(b) At long times both θ_1^* and θ_2^* have the same slope as the ideal-line-source solution θ_0^* and almost coincide with it.

(c) As ω increases, the time at which θ_1^* and θ_2^* become parallel to θ_0^* decreases.

As a further check on the results, the values obtained for θ_1^* were compared with those calculated by Tsymarnyi & Potienko (1976) and were found to be in excellent agreement.

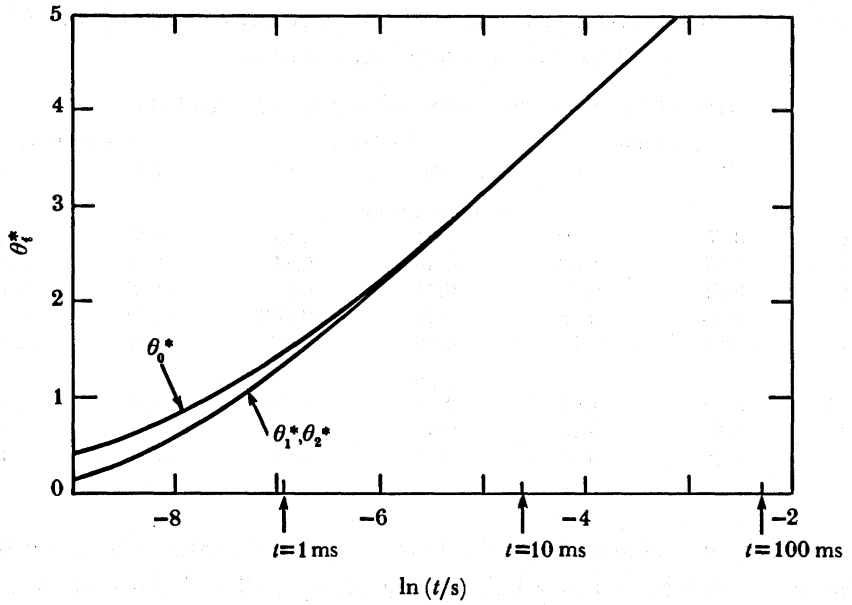

FIGURE 18. Comparison of θ_1^* and θ_2^* with θ_0^* for large ω; $\lambda_f = 0.05$ W m^{-1} K^{-1}, $\omega = 2.0$.

Having established that (5.36) and (5.37) gave identical results over the range of κ_f and ω values found in practice, we compared the values obtained from (5.36) with an analytic approximation of it valid at long times. This approximation is the one used in transient hot-wire experiments to correct for the finite heat capacity of the wire. The approximation is obtained by using an expansion of the Laplace transform of the temperature $\bar{T}_w(p)$, in powers of p and integrating the result term by term. The method is outlined by Carslaw & Jaeger (1959, p. 339). Retaining only the first two terms, the approximation is

$$\theta_a^* = \Delta T_w/(q/4\pi\lambda_f) = \ln(4\kappa_f t/a^2 C)\{1-(a^2/2\lambda_f t)(\rho_w C_{p,w} - \rho_f C_{p,f})\}. \quad (5.38)$$

Note that the leading term on the right-hand side of (5.38) is simply the ideal-line-source solution. This agrees with the previous numerical calculations for long times.

Table 6 summarizes the results of the comparison for two gases, argon and carbon dioxide, at three times (50, 500 and 1000 ms respectively) for a variety of ω values and shows the percentage corrections necessary to bring the actual temperature rise on to the ideal-line-source straight-line solution. A number of trends may be deduced from table 6, including the following.

(*a*) At a given t both corrections decrease with increasing ω and for sufficiently high ω are negative.

(*b*) At constant ω the corrections are nearly constant for $t > 500$ ms. This means θ_1^* and θ_2^* are asymptotically parallel to θ_0^* and in the case of θ_a^* the solutions become coincident.

(*c*) D1 > D2 for all t and ω, where D1 and D2 are percentage differences in temperature between the two approximations and the ideal case.

In the past (Haarman 1969; de Groot *et al.* 1974), the correction for the finite heat capacity of the platinum wire was based on the approximate solution, θ_a^*, valid at long times. The correction procedure would typically be as follows. The raw experimental data, wire-temperature rises and the logarithm of the times, would be assumed to obey the ideal line-source solution, equation (1.8). A least-squares fit yielded the thermal conductivity from the

TABLE 6. PERCENTAGE DIFFERENCE BETWEEN THE IDEAL SOLUTION AND θ_1^2 AND θ_a^* AT THREE TIMES FOR VARIOUS VALUES OF ω

$(D1 = \{(\theta_0^* - \theta_1^*/\theta_0^*)/\theta_0^*\} \times 100;\ D2 = \{(\theta_0^* - \theta_a^*/\theta_0^*\} \times 100.)$

	$t = 50$ ms		$t = 500$ ms		$t = 1000$ ms	
ω	$D1$	$D2$	$D1$	$D2$	$D1$	$D2$
			carbon dioxide			
0.001	3.25	2.40	0.51	0.24	0.38	0.12
0.364	1.57	1.08	0.50	0.11	0.42	0.05
0.951	0.71	0.24	0.41	0.02	0.38	0.01
1.658	0.56	0.06	0.41	0.006	0.39	0.003
3.283	−0.29	−0.71	0.46	−0.07	0.46	−0.04
			argon			
0.0006	2.65	1.97	0.45	0.20	0.34	0.10
0.346	1.17	0.70	0.44	0.07	0.38	0.04
1.277	1.12	0.73	0.53	0.07	0.47	0.04

slope of the plot of $\Delta T_w(a, t)$ against $\ln(t/t^{\circ})$. This approximate value of λ would then be used to calculate the heat capacity corrected rises θ_a^* given by (5.38). Each temperature rise was corrected by an amount $(\theta_a^* - \theta_0^*)$ and the resulting points refitted. The slope of this second line then yielded an improved estimate of the thermal conductivity coefficient. Any point requiring a correction which was greater than a specified limit (usually 0.5 % of the ideal temperature rise) was discarded in the subsequent analysis. The calculations made by using this method show that the true correction is always underestimated, but that the slope of the corrected line is not affected because of (*b*) above. As this is the case then any plots of $\Delta T_w(a, t)_{cor}$ against $\ln(t/t^{\circ})$ will give correct values of the thermal-conductivity coefficient.

It has already been noted that the solutions θ_1^* and θ_a^* are approximately parallel to θ_0^* at sufficiently long times. By setting an upper limit of 0.5 % on the magnitude of the correction and by discarding time points whose magnitude exceed this limit, we find the approximate correction θ_a^* is sufficient for measurements to the precision described in this paper. θ_a^* is also the most obvious choice, purely from ease of computation.

Thus the final form of the correction to be applied may be written as

$$\Delta T_{id}(a, t) = \Delta T_{C,p}(a, t)/C_2(t), \tag{5.39}$$

where

$$C_2(t) = 1 - (a^2/2\lambda_f t)(\rho_w c_{p,w} - \rho_f c_{p,f}). \tag{5.40}$$

ΔT_{id} is the ideal line-source temperature rise and $\Delta T_{C,p}$ is the corresponding temperature rise of a wire acting as a finite segment of an infinite line source with finite heat capacity $c_{p,w}$ and density ρ_w. By making the radius of the hot wire small, about 3.7 μm in our apparatus, the residual uncertainty in $C_2(t)$ is negligible for the range of times of interest.

(*d*) *Finite outer boundary*

Hitherto we have assumed the absence of any physical boundary to the gas medium. This is obviously not the case in a practical cell where there is the mathematically well-defined boundary of the cell wall. In physical terms it turns out that during an experiment the medium at radius $r = a$ does not 'sense' the existence of a boundary at $r = b$ (where b is the cell radius) until the heat flux reaches b and modifies the boundary conditions previously assumed, i.e. $\Delta T = 0$ at $r = \infty$ for all $t > 0$. However, at some time, the fluid at $r = a$ will sense the effect

of the cell boundary and the temperature rise at $r = a$ will be less than that of the ideal case for infinite surroundings, as the heat flux is absorbed into the much more conductive cell walls. Fischer (1939) has investigated this problem and has solved the Fourier equation (1.1) with the modified boundary conditions:

at $r = b$ and $t \geqslant 0$ $$\Delta T(r, t) = 0, \tag{5.41}$$

and at $r = a$ and $t \geqslant 0$ $$\partial T/\partial r = -(q/2\pi a\lambda_f). \tag{5.42}$$

Equation (5.42) avoids the problem of a divergent ratio for b/a. The asymptotic form of the solution is all that is required in this case for $b/a \ll 1$ and $4\tau/a^2 \gg 1$, and this is given by

$$\Delta T_m(a, t) = (q/4\pi\lambda)\left[2\ln(b/a) - \sum_{n=1}^{\infty}\{\exp(-g_n^2\tau/b^2)\}\{\pi Y_0(g_n)\}^2\right]. \tag{5.43}$$

Thus the correction factor $C_3(t)$ to be applied to the ideal case is

$$C_3(t) = \{\Delta T_{id}(a, t)/\Delta T_m(a, t)\}, \tag{5.44}$$

or $$C_3(t) = \ln(4\tau/a^2C)\left[2\ln(b/a) - \sum_{n=1}^{\infty}\{\exp(-g_n^2\tau/b^2)\}\{\pi Y_0(g_n)\}^2\right], \tag{5.45}$$

where g_n is the nth consecutive root of the zeroth-order Bessel function of the first kind and $Y_0(g_n)$ is the zeroth-order Bessel function of the second kind evaluated at g_n; b is the cell outer radius and τ is defined in (5.2). The correction is only significant at long times and only in the order of magnitude range given by

$$2.3 < b^2/\tau < 5.8. \tag{5.46}$$

We also make the practical proviso, as in the case of the heat capacity correction for small times, that any correction larger than 0.5 % of the ideal-line-source temperature rise causes that point to be discarded from all subsequent analysis.

(*e*) *Temperature jump*

Because the hot-wire apparatus uses wires of small diameter, Knudsen effects (Hirschfelder *et al.* 1954) must be taken into account especially at low densities where the mean free path of the molecules is of the same order as the wire diameter. The effect manifests itself by a temperature discontinuity or jump at the wire–fluid interface, with $T_w > T_f$, and it has been reported by Smoluchowski (1911 *a*, *b*). His equation for the temperature difference between wall and fluid, δT_K, is

$$\delta T_K = T_w(a, t) - T_f(a, t) = -g(\partial T/\partial r)_{r=a}, \tag{5.47}$$

where g is a constant called the jump factor. The presence of such a temperature jump modifies the boundary conditions for the Fourier equation at $r = a$ and $t \geqslant 0$ to

$$-2\pi a\lambda_f(\partial T/\partial r)_{r=a} = q. \tag{5.48}$$

Combining (4.51) and (4.52) we obtain

$$\delta T_K = qg/2\pi a\lambda_f. \tag{5.49}$$

Equation (5.49) shows that to a first approximation δT_K is independent of time. Thus, using

(4.53), we can rewrite the line-source solution to include this temperature difference to first order, namely

$$\Delta T_w(a,t) = (q/4\pi\lambda_f)\,(2g/a) + \ln(4\tau/a^2C). \tag{5.50}$$

Reference to figure 19 shows that physically all that has occurred is the vertical displacement of the plot of ΔT_w against $\ln(t)$ without alteration of the slope, from which the thermal

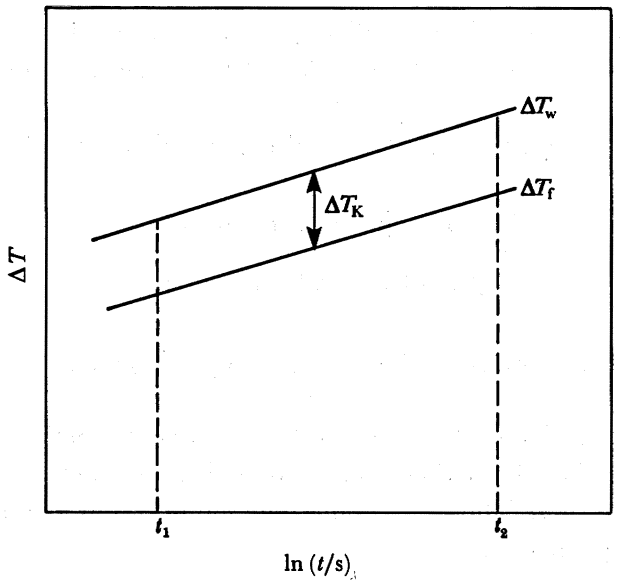

FIGURE 19. First-order Knudsen effect.

conductivity is calculated. So far we have assumed that the temperature jump, thermal conductivity and jump factor g are all independent of temperature. In addition we have assumed that the medium's physical properties are independent of temperature. This is obviously only an approximation over the duration of an experiment.

Allowing the thermal conductivity to be a function of temperature modifies the situation. Because from (5.49) $\delta T_K \propto 1/\lambda_f$, then the following must also hold:

$$\delta T_K \propto 1/\Delta T. \tag{5.51}$$

Figure 20 shows how the above consideration affects the simple first-order analysis of figure 19. The shift in the line is now compounded with a change in slope. The presence of temperature jump thus leads to the line EF with the thermal conductivity of the gas obtained from the slope of EF. However it is the temperature rise of the wire, the line CD, which is measured. It is not difficult to show (Healy *et al.* 1976) to a good approximation that the slope of CD is the same as the slope EF would have if it were at the temperature T_A and not T_B, where T_A and T_B are the mean temperatures taken between the two chosen times, t_1 and t_2, used to evaluate the slope of the straight line. In other words, the variation of thermal conductivity with temperature compensates the effect of temperature jump at the wire–gas interface. Even so, fluid states at sufficiently low pressures, characterized by large Knudsen numbers, must be excluded from our study. In practice this constraint presents no practical difficulties as the lowest pressures used are, for other reasons, much higher than the limit imposed by the Knudsen effects.

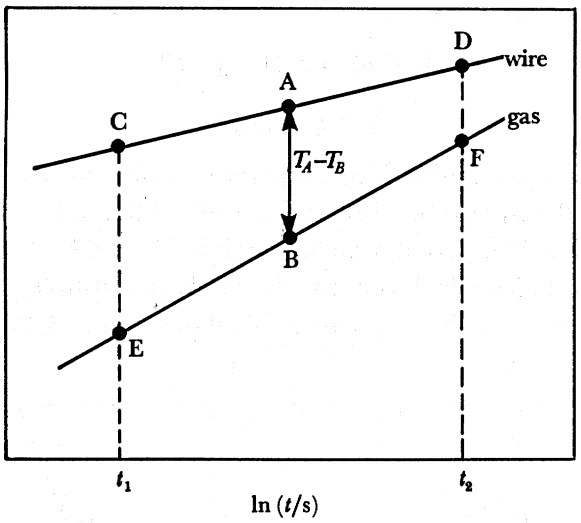

FIGURE 20. Second-order Knudsen effect.

(*f*) *Variable fluid properties*

We have supposed so far that the basic solution to the line-source equation contains only temperature-independent parameters, with the exception of the preceding section on temperature jump when the thermal conductivity was considered to be a linear function of temperature. We now discuss the general effects of the variation of thermal conductivity and density with temperature on the transient hot-wire experiment. These properties are considered to be weak linear functions of temperature, a reasonable approximation over the small temperature rise of a hot-wire experiment (*ca.* 7 K). Variation of fluid properties has effects of two types. Firstly, variations in density causes motion of the gas, which is discussed in the next section. Secondly, variations in both properties complicate the equations previously derived and this will be discussed below.

Following the analysis of Healy *et al.* (1976), we now assume linear dependence of thermal conductivity and density on temperature. The heat capacity is much less temperature dependent and is thus considered constant over the small temperature rises used in the hot-wire experiment, provided that the experiment is not carried out too near the critical point. The Fourier equation is once again solved and a solution found as a perturbation on the ideal-line-source, temperature-independent, fluid-properties case. The solution obtained is in the form of a correction term δT to the ideal line source by iteration, namely

$$\Delta T^{(2)} = \Delta T_{\mathrm{id}} + \delta T, \tag{5.52}$$

or

$$\Delta T^{(2)} = \frac{q}{4\pi\lambda_t}\ln\left(\frac{4\tau}{a^2C}\right) - \left[0.5 - \frac{(1-\phi/\chi)\ln 4}{\{\ln(4\tau t/a^2C)\}^2}\right]\chi(\Delta T)^2. \tag{5.53}$$

The parameters ϕ and χ are defined from the following equations:

$$\rho = \rho_0(1+\phi\Delta T), \tag{5.54}$$

and

$$\lambda(T,\rho) = \lambda_0(1+\chi'\Delta T+\gamma\Delta p). \tag{5.55}$$

Combining (5.54) and (5.55) gives

$$\lambda(T,\rho) = \lambda_0(1+\chi\Delta T), \tag{5.56}$$

where

$$\chi = \chi' + \gamma\rho_0\phi, \tag{5.57}$$

and the subscript 0 refers to the equilibrium temperature before the transient heating. In (5.53) the second term within the square brackets is generally of the order of 0.05 and thus may be ignored with respect to 0.5. The second term on the right-hand side of (5.53) causes a curvature in the plot of ΔT against $\ln(t)$, which is normally barely perceptible, except when the critical point is approached. Figure 21 shows a curve calculated from (5.53) for CO_2 at 316 K, or

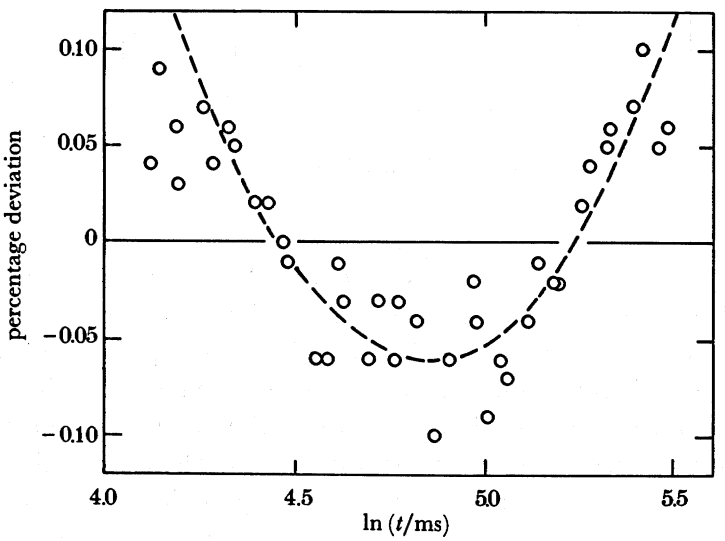

FIGURE 21. Percentage deviations of the temperature rise of the wire, ΔT, from a best fit of a linear relation between ΔT and $\ln(t)$ the logarithm of time. The broken line is the curve from equation (5.53); o are experimental points.

about 12 K above the critical temperature, and close to the critical density. For this system, $\lambda_f = 67.60$ mW m^{-1} K^{-1}, $\chi = 0.0137$ and the other parameters are values used in the apparatus described below. The timescale shown is from 50 to 270 ms. The percentage deviations of the temperature rise due to the effect of the variation of λ_f are shown and can be seen to be small even under these extreme conditions. Also shown are some experimental points (Scott *et al.* 1983).

The average slope of this line of ΔT_w against $\ln(t)$ is given by

$$\frac{\Delta T(t_2)-\Delta T(t_1)}{\ln(t_2/t_1)} = \left[\frac{q/4\pi\lambda_0}{1+(\chi/2)\{\Delta T(t_1)+\Delta T(t_2)\}}\right]. \tag{5.58}$$

Equation (5.58) is identical to a line-source solution with fluid properties evaluated at

$$T_r = \tfrac{1}{2}\{\Delta T(t_1)+\Delta T(t_2)\}+T_0, \tag{5.59}$$

and

$$\rho_r = \rho(T_r, P_0). \tag{5.60}$$

Thus the slope of the measured line of temperature rise against $\ln(t)$ determines the thermal conductivity not at the equilibrium temperature of the ambient experimental conditions, but

at some reference temperature calculated from (5.59) and at a reference density given by (5.60), at the essentially constant pressure P_0. Thus the temperature dependence of the thermal conductivity and density of the fluid is reflected in the reference state of the fluid to which the measured value of the thermal conductivity is assigned.

(g) *Convection and other gas dynamic effects*

Consider now the case of variable density in an infinite fluid medium with an infinite line source. The transient heating of the hot wire induces density variations which in a gravitational field produce buoyancy forces leading to convective motion. The convective motion of the fluid has two components: one due to radial temperature gradients and one due to axial temperature gradients at the ends of the wires. The experimental onset of convection can be observed directly in the hot-wire experiment by noting the departure of the temperature rise from the fundamental equation (1.8) at long times. As long as no departure from the ideal case can be discerned the thermal conductivity measurements will not include a significant convective component. Estimates of the onset times for both types of convection can be made as follows.

Convection due to the radial temperature gradient in this type of experiment has been discussed by Van der Held & Van Drunen (1949), Falcao (1967) and Vilcu & Ciochina (1981). The equations they use are based on the following inequality for the absence of free convection.

$$Ra = \frac{g\beta_t \rho_t^2 c_p \Delta T d^3}{\eta \lambda_t} \leqslant 1000, \tag{5.61}$$

where Ra is the Rayleigh number, g is the acceleration due to gravity, β_t is the thermal expansion coefficient of the fluid, η its dynamic viscosity and d a distance over which a temperature rise ΔT occurs. This will be the distance between the wire and the edge of the thermal wave moving out into the medium. A value for d can be obtained by setting ΔT_{id} in (1.8) to zero when r will be given by

$$r = \sqrt{(4\lambda_t t / C\rho_t c_p)}, \tag{5.62}$$

where C is defined in (1.9), and so we can take

$$d = \sqrt{(4\lambda_t t / C\rho_t c_p)} - a. \tag{5.63}$$

The condition for the onset of free convection then becomes

$$1000 = \frac{g\beta_t \rho_t^2 c_p \Delta T}{\eta \lambda_t} \{\sqrt{(4\lambda_t \bar{t} / C\rho_t c_p)} - a\}^3, \tag{5.64}$$

where $\bar{t}$ is the onset time for convection, or

$$\bar{t} = \frac{0.445 \rho_t c_p}{\lambda_t} \left\{ \left(\frac{1000 \eta \lambda_t}{g\beta_t \rho_t^2 c_p \Delta T} \right)^{\frac{1}{3}} + a \right\}^2. \tag{5.65}$$

Typically a is small compared to the previous term in the brace and so

$$\bar{t} \approx 44.5 \left(\frac{\eta^2 c_p}{g^2 \beta_t^2 \rho_t \lambda_t \Delta T^2} \right)^{\frac{1}{3}}. \tag{5.66}$$

Onset times calculated from (5.66) with typical experimental parameters are normally in excess of the maximum times used for experimental measurement, i.e. 2 s or greater. If

conditions are deliberately chosen so that convection occurs within the measurement period, (5.66) appears to predict quite accurately the onset time. Table 7 shows the results of experiments on ammonia at 383 K at a density of 41 kg m^{-3} with an excessive temperature rise of 10 K. The table shows percentage deviations of measured ΔT values from a straight line of ΔT against ln (t) fitted to the first six points indicating that convection begins to occur between 393 and 478 ms. Equation (5.66) predicts a value for $\bar{t}$ of 402 ms.

TABLE 7. DEVIATIONS OF THE MEASURED VALUES OF ΔT FROM A STRAIGHT-LINE FIT OF ΔT AGAINST $\ln t$ FOR THE FIRST SIX POINTS: THE RESULTS ARE FOR AMMONIA AT 383 K AND 41 kg m^{-3}

t/ms	ln (t/ms)	ΔT/K	dev. (%)
160	5.0766	8.3278	−0.01
191	5.2536	8.4879	0.00
228	5.4305	8.6491	0.02
274	5.6164	8.8139	−0.00
330	5.8011	8.9791	0.01
393	5.9768	9.1387	0.00
478	6.1718	9.3078	−0.12
577	6.3601	9.4737	−0.20
702	6.5550	9.6396	−0.33
859	6.7577	9.8070	−0.53
1073	6.9798	9.9744	−0.90
1526	7.3326	10.1420	−2.47

Convection effects due to axial temperature gradients at the ends of the wire are now considered. The resultant convective motion causes upward acceleration of fluid near the wire and cooler fluid from below is brought upwards cooling the wire faster than by radial conduction alone. The transition to convective heat transfer at some point along the wire begins only when some effect from the end of the wire has propagated to that point. Although the inertia of the fluid delays this propagation, the flow pattern will eventually establish itself over a sufficient length of wire to affect the temperature rise. The treatment by Goldstein & Briggs (1964) suggests that the characteristic time, $\bar{t}$, before which convective effects may be neglected is given by

$$\bar{t} = (l\lambda/0.32g\beta_t q)^{\frac{1}{2}}, \tag{5.67}$$

where l is the wire length, g is the acceleration due to gravity, β_t is the coefficient of thermal expansion of the fluid, and q is the heat generated per unit length by the hot wire. Equation (5.67) is not precise but serves as a useful starting point for design. For fluids removed from their critical point, $\bar{t}$ is about 3 s for gases and about 5 s for liquids (Wakeham 1979). Vertical convection effects are also reduced by subtracting the effects in the long and short wires and in any case are again observable experimentally.

In addition to convection, a second dynamic effect results from the finite volume of gas in the system. Addition of heat to a system of fixed mass m and volume V causes the pressure to increase with time. The expanding boundary layer can be imagined to perform expansion work on the remaining gas in the cell. This causes the background temperature in the cell to increase slowly with time. This modifies the equilibrium temperature T_0 so that at any instant

$$T' = T_0 + \delta T_c, \tag{5.68}$$

where δT_c is obtained by disregarding all heat losses from the cell and is given by

$$\delta T_c \approx qlRt/(\rho_f c_p c_v V), \tag{5.69}$$

where R is the gas constant, l is the wire length, ρ_f is the fluid density, c_p and c_v are the molar heat capacities at constant pressure and volume respectively, and V is the volume of the container.

Equation (5.69) shows that if V is large enough then δT_c can be neglected. We can verify experimentally whether this is justified by noting if a different result is obtained when an additional volume of gas is coupled to the cell. Because δT_c is inversely proportional to density, the test should be carried out at the lowest operating pressure. In practice it is found that δT_c cannot be neglected below a low pressure limit of about 0.5 MPa for most gases, which is not a severe restraint.

(*h*) *Radiation effects*

The other mode of heat transfer possible as the line source heats up is by radiation to the surrounding medium. It has two effects. Firstly, there is a direct effect of the energy lost that would otherwise be dissipated by conduction. Secondly, any element in the medium may partly absorb the radiation, thereby changing its temperature so that it will be different from that of the pure conduction case. The same fluid element subsequently emits some of the radiation to other fluid elements. Thus the slower thermal conduction wave-front, spreading out from the hot wire, encounters fluid not at the equilibrium temperature at which the transient was initiated. The temperature history of the wire is therefore affected directly through radiative heat loss and indirectly by way of absorption in the fluid.

Most gases of up to moderate densities are assumed to be transparent to radiation. This being the case, it is easy to determine the amount of heat radiated per unit length of the hot wire, q_{rad}, namely

$$q_{rad} = 2\pi a \sigma_B (T_w^4 - T_0^4), \tag{5.70}$$

where σ_B is the Stefan–Bolzmann constant and a the wire radius. Here we have also assumed that the wire radiates in a similar fashion to a black body. Equation (4.70) can be approximated to

$$q_{rad} = 8\pi a \sigma_B T_0^3 \Delta T_w, \tag{5.71}$$

assuming that the temperature difference between wire and fluid is small. The modification to the temperature rise of the wire is only 0.02 % for platinum wires of the dimensions used here, and is approximately given by

$$\delta T_{rad} = (q_{rad}/q)\,\Delta T(a,t) = (8\pi a \sigma_B T_0^3/q)\{\Delta T(a,t)\}^2. \tag{5.72}$$

The more difficult general case of partial absorption of the radiative heat flux has been studied numerically by Saito & Venart (1978). Wakeham (1979) suggests that for liquids of intermediate optical density, the radiative contribution may be as much as 0.3 % of the measured thermal conductivity. However, pending a more accurate solution, this would better be considered a residual systematic error in the thermal-conductivity measurement.

(*i*) *Mixtures*

For any system, the steady-state thermal conductivity is defined by Fourier's phenomenological equation for the heat flux

$$q = -\lambda_\infty \nabla T. \tag{5.73}$$

PHILOSOPHICAL TRANSACTIONS OF THE ROYAL SOCIETY A MATHEMATICAL, PHYSICAL & ENGINEERING SCIENCES

In equation (5.73), λ is the thermal conductivity of the fluid mixture and the subscript ∞ denotes steady state. However, for mixtures in the steady state, a concentration gradient is also established by thermal diffusion, where there is no net mass flux of any species. This is in direct contrast to the transient condition where no such concentration gradient exists and the composition is assumed to be uniform. At $t > 0$ in the transient case we can write

$$q = -\lambda_t \Delta T, \tag{5.74}$$

where the subscript on λ refers to the case of uniform composition. In the case of dilute gas mixtures, λ_∞ and λ_t may differ by up to several per cent (Wakeham 1979) and so it is important to discover which of the two is measured in the transient hot-wire experiment. An analysis of a binary mixture of perfect gases subject to transient heating by a line source has been carried out by Khalifa *et al.* (1979). The result, expressed as the temperature rise of the wire, is

$$\Delta T_{\mathrm{id}} = (q/4\pi\lambda_\infty) \ln (\kappa' t/a^2 C), \tag{5.75}$$

where κ' is a time-independent quantity that is a function of the thermal-diffusion factor and diffusion coefficient in addition to the thermal diffusivity. The mass fluxes, therefore, produce a parallel shift of the $\{\Delta T, \ln (t)\}$ plot relative to the line for a pure gas with the same physical properties of the mixture. However, the thermal conductivity is the same as that determined from steady-state considerations. This can be rationalized by examining the boundary conditions at the hot-wire surface. At the surface there is no mass transfer into the wire so there is no net mass flux, which corresponds to the steady-state situation.

(*j*) *Temperature coefficient of wire resistance*

To translate the measured changes in resistance of the platinum wire into temperature rises it is necessary to know accurately its resistance–temperature relation. The temperature coefficient of the resistivity of the wire is obtained by measuring the resistance of a wire at a number of temperatures. However, the geometry of the wires will change during an experiment because of thermal expansion. To take this into account we need also to consider the effect of tension on the wire resistances. Following the work of Clifford *et al.* (1980*b*), we consider first the effect on its resistance of subjecting a wire of length l_0 to an axial force F, which is less than its ultimate tensile strength. Young's modulus E for the wire is defined by

$$E = (F/A_0)/(\epsilon_{\mathrm{w}}/l_0), \tag{5.76}$$

where A_0 is the cross-sectional area of the unloaded wire and ϵ_{w} is the extension of the wire. Rearranging we obtain

$$X = F/A_0 E, \tag{5.77}$$

where

$$X = \epsilon_{\mathrm{w}}/l_0. \tag{5.78}$$

At the same time the cross-sectional area, A_0, of the wire will fall by an amount, δA_0, given by Poisson's ratio, ν, in the formula

$$\delta A_0/A_0 = 2\nu X. \tag{5.79}$$

The resistance of the wire under zero tension is given by

$$R(O, T) = \rho l_0/A_0, \tag{5.80}$$

where ρ is the electrical resistivity. Under tension T,

$$R(F, T) = \rho(l_0+\epsilon_w)/(A_0-\delta A_0) \tag{5.81}$$

$$= R(O, T)(1+X)(1-2\nu X)^{-1} \tag{5.82}$$

$$\approx R(O, T)\{1+(1+2\nu)X\} \tag{5.83}$$

neglecting terms in X higher than the first power.

Substituting for X from (5.77) gives

$$R(F, T) = R(O, T)\{1+(2\nu+1)(F/A_0 E)\}. \tag{5.84}$$

This will occur during an experiment because of changes in the wire temperature and will change the effective temperature coefficient of resistance. The schematic diagram of a wire and spring under tension is shown in figure 22. Here, l_0 and h_0 are the original lengths of the wire and spring and ϵ_w and ϵ_s their extensions under tension. C_0 is the total length, where

$$C_0 = l_0+\epsilon_w+h_0+\epsilon_s. \tag{5.85}$$

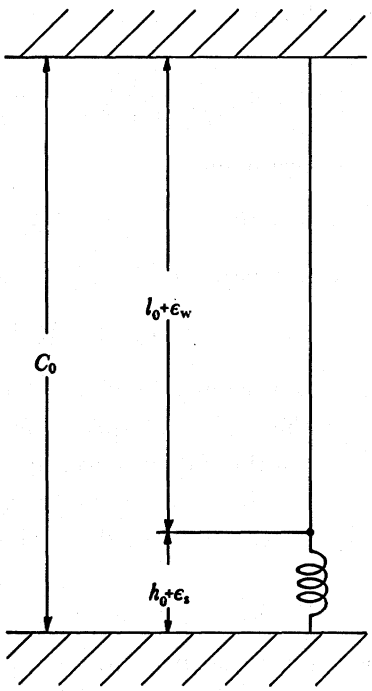

FIGURE 22. Schematic diagram of wire tensioning.

Also, ϵ_w and ϵ_s can be related to the tension via the force constants k_w and k_s thus

$$\epsilon_w = k_w F, \quad \epsilon_s = k_s F, \tag{5.86}$$

and therefore

$$F(1/k_w+1/k_s) = C_0-l_0-h_0. \tag{5.87}$$

If the wire is under constant tension the resistance would change as follows, if the temperature is raised by δT,

$$R \to R(1+\alpha_0 \delta T), \tag{5.88}$$

where α_0 is the temperature coefficient of resistance. However, in an experiment the wire expands and the following changes take place

$$\left.\begin{aligned} l_0 &\to l_0(1+\beta_w \delta T), \\ F &\to F+\delta F, \\ R &\to R(1+\alpha_e \delta T). \end{aligned}\right\} \quad \text{and} \tag{5.89}$$

In (5.89), β_w is the linear coefficient of expansion of the wire material, δF is the change in tension and α_e the effective temperature coefficient of resistance.

From equations (5.84), (5.88) and parts of (5.89), the difference in resistance change can be related to the change in tension

$$R(\alpha_e \delta T - \alpha_0 \delta T) = R(2\nu+1)\,\delta F/(A_0 E). \tag{5.90}$$

It remains to obtain an expression for δF, which can be obtained from (5.87) and (5.89),

$$\delta F(1/k_w + 1/k_s) = l_0 \beta_w \delta T. \tag{5.91}$$

Combining (5.90) and (5.91) we obtain

$$\alpha_e - \alpha_0 = \frac{l_0 \beta_w (2\nu+1)}{(1/k_w + 1/k_s)(A_0 E)}. \tag{5.92}$$

Using the following experimental parameters

$$l_0 = 0.16 \text{ m}, \quad \beta_w = 16\times10^{-6}\,\text{K}^{-1}, \quad \nu = 0.5, \quad k_w = 40.4 \text{ N m}^{-1},$$
$$k_s = 1 \text{ N m}^{-1}, \quad A_0 = 8.848\times10^{-11}\,\text{m}^2, \quad E = 1.68+10^{11}\,\text{Pa},$$

we obtain

$$\alpha_e - \alpha_0 = -0.34\times10^{-6}\,\text{K}^{-1},$$

giving a difference of 0.01 % in a typical value of α of *ca.* $0.4\times10^{-3}\,\text{K}^{-1}$. The calculation above ignores the effects of the mass of the wire and spring and also that the spring-extension characteristics may differ from those of the bulk material because of internal strain. However, these should not affect the order of magnitude of the result. It can readily be shown, in the case of the apparatus described here, that the mass of the spring has a 25 % effect on the wire tension.

(*k*) *Summary of corrections*

It is found that the major corrections that need to be applied to the data from a transient hot wire arise from (*a*) the finite length of the wire, which is corrected for experimentally by having two wires of different lengths, but which necessitates a further correction for different average values of the resistance per unit length of the two wires; (*b*) the finite heat capacity of the wire, which is especially important at short times; and (*c*) the existence of the outer boundary of the cell, which is especially important at long times. In addition, the value of the thermal-conductivity coefficient obtained is associated with a reference temperature that is the average temperature at which measurements are made. All other corrections can be neglected except that a time-bias correction is applied to correct for the effect of electrical noise as detailed in §3 and the experiment must be carried out before convection begins to occur. An appropriate correction sequence in a typical experiment is detailed below. The corrections $\Delta T^{(i)}$ to the

measured temperature rise ΔT_m are given below, where the superscript indicates the ith correction.

(i) The initial value for the thermal conductivity and thermal diffusivity of the fluid is obtained from the slope of the centre portion of the curve of ΔT_m against $\ln(t)$ for the raw data.

(ii) The measured temperature rises ΔT_m are corrected for the differences in the resistances per unit length by the following equation,

$$\Delta T^{(1)}(t) = \Delta T_m(t)/C_1(t). \tag{5.93}$$

The correction factor $C_1(t)$ is given by

$$C_1(t) = 1 + [R_S(t_0)/R_w(T_0)]\,\epsilon', \tag{5.94}$$

where
$$\epsilon' = \epsilon[1 - \{\ln(4\tau/a^2C)\}^{-1}], \tag{5.95}$$

and
$$\epsilon = 1 - (\sigma_2/\sigma_1). \tag{5.96}$$

(iii) The corrected temperature rises and corresponding times are again subjected to a linear least-squares analysis, and improved values for the thermal conductivity and thermal diffusivity are extracted from the slope.

(iv) Each temperature rise is corrected again for the finite heat capacity of the wire according to

$$\Delta T^{(2)}(t) = \Delta T^{(1)}(t)/C_2(t), \tag{5.97}$$

where
$$C_2(t) = 1 - (a^2/2\lambda_f t)\,(\rho_w c_{p,w} - \rho_f c_{p,f}). \tag{5.98}$$

Any points where the correction is greater than 0.5 % of the temperature rise are discarded in the subsequent analysis.

(v) Step (iii) is repeated.

(vi) The outer boundary correction is applied to each $\Delta T^{(2)}(t)$ according to

$$\Delta T^{(3)}(t) = \Delta T^{(2)}(t)\, C_3(t), \tag{5.99}$$

where
$$C_3(t) = \frac{\ln(4\tau/a^2C)}{2\ln(b/a) - \sum_{n=1}^{30} \{\exp(-g_n^2\tau/b^2)\}\{\pi Y_0(g_n)\}^2}. \tag{5.100}$$

In the summation only 30 roots of the Bessel functions are considered as they generally converge very rapidly for gases. Once again any points that have a correction greater than 0.5 % of the temperature rise, are discarded from further analysis.

(vii) Step (iii) is repeated to give a final value for the thermal conductivity and thermal diffusivity. The thermal conductivity extracted is then associated with a reference temperature and density given by

$$T_r = \tfrac{1}{2}\{\Delta T(t_i) + \Delta T(t_f)\} + T_0, \tag{5.101}$$

and
$$\rho_r = \rho(T_r, P_0), \tag{5.102}$$

where t_i and t_f are the first and last times to be included in the final least-squares fitting procedure. T_0 and P_0 are the initial equilibrium temperature and pressure before the run.

6. Error analyses

Errors in the apparatus may be divided into three categories: (*a*) model errors due to the assumption of a particular mathematical model to represent the system; (*b*) systematic errors in the measurements due to unknown factors; and (*c*) random statistical errors in the measured input variables for the mathematical model.

Categories (*a*) and (*b*) above are dealt with first. Healy *et al.* (1976) have shown that, with the corrections discussed in this section, the line-source solution is an excellent model for the behaviour of hot-wire apparatus. The systematic errors can be judged by comparison with data obtained from other methods, in particular by comparing the measured values of thermal conductivity at zero density with those derived from viscosity data. The differences so obtained give a good guide to the magnitude of the systematic errors in the apparatus. The third category is tackled in the following section.

(*a*) *Parameter-variation calculations*

The thermal conductivity obtained from an individual run can be regarded as a function of the independent measured input variables

$$\lambda = \lambda(a, t, \alpha, R_{\mathrm{L}}, R_{\mathrm{S}}, l_1, l_2, \rho_{\mathrm{f}}, c_{\mathrm{p,f}}, R_1, R_2). \tag{6.1}$$

We postpone discussion of the errors in the measurement of time until the next section. Let δx be the uncertainty in variable x, then $\delta\lambda$ the uncertainty in thermal conductivity (not including the effect of time) is given by

$$\begin{aligned}\langle\delta\lambda\rangle^2 = {} & \left(\frac{\partial\lambda}{\partial a}\right)^2\langle\delta a\rangle^2 + \left(\frac{\partial\lambda}{\partial\alpha}\right)^2\langle\delta\alpha\rangle^2 + \left(\frac{\partial\lambda}{\partial R_{\mathrm{L}}}\right)^2\langle\delta R_{\mathrm{L}}\rangle^2 + \left(\frac{\partial\lambda}{\partial R_{\mathrm{S}}}\right)^2\langle\delta R_{\mathrm{S}}\rangle^2 \\ & + \left(\frac{\partial\lambda}{\partial R_1}\right)^2\langle\delta R_1\rangle^2 + \left(\frac{\partial\lambda}{\partial R_2}\right)^2\langle\delta R_2\rangle^2 + \left(\frac{\partial\lambda}{\partial l_1}\right)^2\langle\delta l_1\rangle^2 \\ & + \left(\frac{\partial\lambda}{\partial l_2}\right)^2\langle\delta l_2\rangle^2 + \left(\frac{\partial\lambda}{\partial c_{\mathrm{p}}}\right)^2\langle\delta c_{\mathrm{p}}\rangle^2 + \left(\frac{\partial\lambda}{\partial\rho c_{\mathrm{p}}}\right)^2\langle\delta\rho c_{\mathrm{p}}\rangle^2.\end{aligned} \tag{6.2}$$

Let us simplify this equation by assuming that some of the uncertainties are identical, i.e.

$$\delta R_{\mathrm{L}} = \delta R_{\mathrm{S}} = \delta r, \quad \delta R_1 = \delta R_2 = \delta R, \quad \delta l_1 = \delta l_2 = \delta l, \tag{6.3}$$

then

$$\begin{aligned}\langle\delta\lambda\rangle^2 = {} & \left(\frac{\partial\lambda}{\partial a}\right)^2\langle\delta a\rangle^2 + \left(\frac{\partial\lambda}{\partial\alpha}\right)^2\langle\delta\alpha\rangle^2 + \left(\frac{\partial\lambda}{\partial c_{\mathrm{p}}}\right)^2\langle\delta c_{\mathrm{p}}\rangle^2 + \left(\frac{\partial\lambda}{\partial\rho c_{\mathrm{p}}}\right)^2\langle\delta\rho c_{\mathrm{p}}\rangle^2 \\ & + \left(\frac{\partial\lambda}{\partial R_{\mathrm{L}}}\right)^2 + \left(\frac{\partial\lambda}{\partial R_{\mathrm{S}}}\right)^2\langle\delta r\rangle^2 + \left(\frac{\partial\lambda}{\partial R_1}\right)^2 \\ & + \left(\frac{\partial\lambda}{\partial R_2}\right)^2\langle\delta R\rangle^2 + \left(\frac{\partial\lambda}{\partial l_1}\right)^2 + \left(\frac{\partial\lambda}{\partial l_2}\right)^2\langle\delta l\rangle^2.\end{aligned} \tag{6.4}$$

To obtain representative values a calculation has been carried out for argon at 76 °C and 15 MPa and the following results were obtained.

$$\left.\begin{aligned}
(\partial\lambda/\partial a)^2 &= 6.25\times10^{8}\ (\mathrm{mW\ m^{-2}\ K^{-1}})^2,\\
(\partial\lambda/\partial\alpha)^2 &= 2.70\times10^{7}\ (\mathrm{mW\ m^{-1}})^2,\\
(\partial\lambda/\partial c_p)^2 &= 10^{-8}\ (\mathrm{mW\ m^{-1}\ J^{-1}\ kg})^2,\\
(\partial\lambda/\partial\rho c_p)^2 &= 1.3\times10^{-8}\ (\mathrm{mW\ m^{2}\ kg^{-1}\ K^{-1}})^2,\\
(\partial\lambda/\partial R_L)^2 &= 4.84\times10^{-2}\ (\mathrm{mW\ m^{-1}\ K^{-1}\ \Omega^{-1}})^2,\\
(\partial\lambda/\partial R_S)^2 &= 1.06\times10^{-1}\ (\mathrm{mW\ m^{-1}\ K^{-1}\ \Omega^{-1}})^2,\\
(\partial\lambda/\partial R_1)^2 &= 2.50\times10^{-3}\ (\mathrm{mW\ m^{-1}\ K^{-1}\ \Omega^{-1}})^2,\\
(\partial\lambda/\partial R_2)^2 &= 4.23\times10^{-3}\ (\mathrm{mW\ m^{-1}\ K^{-1}\ \Omega^{-1}})^2,\\
(\partial\lambda/\partial l_1)^2 &= 1.37\times10^{5}\ (\mathrm{mW\ m^{-2}\ K^{-1}})^2,\\
\text{and}\quad (\partial\lambda/\partial l_2)^2 &= 1.37\times10^{5}\ (\mathrm{mW\ m^{-2}\ K^{-1}})^2.
\end{aligned}\right\}\qquad (6.5)$$

The uncertainties in the independent parameters have been assigned the following values based on experience.

$$\langle\delta\alpha\rangle = \pm10^{-5}\ \mathrm{K^{-1}}$$

$$\langle\delta a\rangle = \pm2\times10^{-7}\ \mathrm{m^{-1}}$$

$$\langle\delta c_p\rangle = \pm60\ \mathrm{J\ kg^{-1}\ K^{-1}}$$

$$\langle\delta\rho\rangle = \pm20\ \mathrm{kg\ m^{-3}}$$

$$\langle\delta r\rangle = \pm0.05\Omega$$

$$\langle\delta R\rangle = \pm0.1\Omega$$

$$\langle\delta l\rangle = \pm5\times10^{-5}\ \mathrm{m}.$$

Substituting these uncertainties into (6.4) leads to the following table, which shows the contribution of each uncertainty in the independent parameters to the mean squared error in thermal conductivity.

δx	$\dfrac{\langle\delta x\rangle^2(\partial\lambda/\partial x)^2}{(\mathrm{mW\ m^{-1}\ K^{-1}})^2}$	order of importance
δa	2.70×10^{-3}	1
δl	6.85×10^{-4}	2
δr	3.80×10^{-4}	3
δR	6.73×10^{-5}	4
δc_p	3.6×10^{-5}	5
δa	2.5×10^{-5}	6
$\delta\rho$	5.2×10^{-6}	7
$\langle\delta\lambda\rangle^2$	3.9×10^{-3}	—

From the last line of the table we deduce that $\langle\delta\lambda\rangle = 0.06\ \mathrm{mW\ m^{-1}\ K^{-1}}$, and because for this example $\lambda = 25.96\ \mathrm{mW\ m^{-1}\ K^{-1}}$ this represents a percentage uncertainty of 0.24 %. Inspection of the terms in the table shows that the major contribution to the random error is the uncertainty in α for the wires followed by the uncertainties in their lengths and equilibrium resistances.

(*b*) *Time errors*

Until now we have ignored random errors in the time measurement, although the times must be corrected for bias (§3). The final thermal conductivity is obtained from a linear least-squares analysis on the set of between 9 and 12 $\{\ln(t/t^{\circ}), \Delta T\}$ values, obtained during a run, by using the following equations:

$$y_t = Ax_t + B,$$

where

$$y_t = (C_3 \Delta T_m / C_1 C_2),$$

$$x_t = \ln(t/t^{\circ}), \tag{6.6}$$

$$A = Q/(4\pi l \lambda_t),$$

and

$$B = A \ln(4\kappa_t t^{\circ}/a^2 C).$$

The y_t are the final corrected temperature rises and the x_t are the natural logarithms of the corrected times. The slope of the regression line together with the calculated heat dissipation in the wire enables the thermal conductivity to be calculated.

In a least-squares analysis the weighted sum of the squares of the differences is minimized. In the absence of other evidence we have so far assumed equal errors in the y_t and zero error in the x_t. To show that the second assumption is not true we only need to look at the random errors in the time interval measurements. These are given in column 3 of table 5 as a function of the voltage rise across the bridge and bridge noise levels. It can be seen that the standard deviations of the time intervals increase with decreasing voltage rise across the bridge.

The time of the rth cross-over is obtained by summing the time intervals from Δt_1 to Δt_r, counting the start of the run as the zeroth cross-over. Thus

$$t_r = \sum_{t=1}^{r} \Delta t_t. \tag{6.7}$$

The variance of the rth point is given by

$$\sigma^2(t_r) = \sigma^2(\Delta t_r). \tag{6.8}$$

This is so because there is negligible delay in switching from one time interval to the next, and thus it is only the error associated with the last interval which determines the overall variance.

Table 8 shows the percentage random uncertainty in the rth time interval as a function of time for a run on argon. The last two columns of table 8 express this uncertainty as a percentage of the total time and as the equivalent percentage uncertainty of the natural logarithm of the times. It is easy to see that for all the times of interest the percentage uncertainty in the x_t defined by (6.6) is negligible and our original assumption of zero errors in the time is seen to be vindicated.

(*c*) *Measurement of thermal diffusivity*

It may be noted that, in principle, equation (6.6) enables the thermal diffusivity to be recovered from the intercept, B, of the linear fit. However, to obtain a reasonable accuracy in the diffusivity, say 1 %, it can be shown that it is necessary to know the absolute temperatures of the hot wires to within several millikelvin. This, in turn, implies a combined accuracy of better than $\pm 0.05\,\Omega$ in the bridge resistances. This figure cannot be met in the present apparatus because of the uncertainties in the resistances of the springs and leads that

TABLE 8. PERCENTAGE UNCERTAINTIES IN THE OBSERVED TIMES DUE TO RANDOM ERRORS IN THE MEASURED TIME INTERVALS FOR ARGON AT 15.15 MPa AND 69.62 °C

r	slope / V s^{-1}	Δt_r / ms	$\sigma(t_r) = \sigma(\Delta t_r)$ / ms	t_r / ms	$\frac{\sigma(t_r)}{t_r}$ (%)	$\frac{\sigma(\ln t_r)}{\ln t_r}$ (%)
1	0.019	85.01	0.13	85.01	0.15	0.03
2	0.019	18.27	0.13	103.28	0.13	0.03
3	0.016	22.33	0.14	125.61	0.11	0.02
4	0.013	27.56	0.16	153.17	0.10	0.02
5	0.010	34.21	0.18	187.38	0.09	0.02
6	0.008	41.26	0.30	278.64	0.11	0.02
7	0.007	53.00	0.50	281.64	0.18	0.03
8	0.005	64.61	0.84	346.25	0.24	0.04
9	0.004	78.49	1.06	424.74	0.25	0.04
10	0.0035	99.66	1.20	525.40	0.23	0.04
11	0.0029	122.54	1.55	646.94	0.24	0.04
12	0.0023	153.17	1.60	800.11	0.20	0.03

respectively tension and connect the platinum filaments. For the measurement of thermal conductivity only, these resistances are not so critical, because it is the gradient, A, in (6.6) that is required and the relative position of the line of $\{\ln(t/t^{\circ}), \Delta T\}$ in relation to the temperature axis does not contribute to an error in this value. Also during a transient run the lead and spring resistances are effectively constant.

A further factor that prevents the measurement of accurate diffusivities is the method of operating the bridge during an experiment. The resistances of the long and short wires are measured before a run, with the bridge in a manual mode. During this measurement, the variable resistance boxes R_1 and R_2 are operated. On completion of these equilibrium measurements, the two resistance boxes are reset to their run positions. At this point the contact resistances in the resistance boxes will not be, in general, the same as when the equilibrium measurements were made, thus contributing to the uncertainties in the absolute resistance of the wires during a run.

A new bridge, with more advanced electronics, is being developed at the National Engineering Laboratory. This bridge is designed to overcome the problem of changing contact resistances and it is hoped will enable diffusivities to be obtained with moderate accuracy.

(*d*) *Weights in the least-squares analysis*

Unit weight was assumed for each y_i but this is incorrect. From (6.6), y_i is a function not only of the measured temperature rise but also the correction factors C_1, C_2 and C_3.

It was shown in §5 that the heat-capacity correction C_2, the largest of the three terms, is only an approximation, which is less good at small times (hence the 0.5 % cut-off factor) and breaks down completely at very small times. With this in mind it would seem reasonable to suppose that the errors in y_i were proportional to the inverse of the percentage correction for C_2. Incorporating such a weighting scheme in the calculations did not alter the results significantly and on that basis it was decided to retain the original system of unit weights.

PHILOSOPHICAL TRANSACTIONS OF THE ROYAL SOCIETY A MATHEMATICAL, PHYSICAL & ENGINEERING SCIENCES

7. Experimental results

(a) *Results for helium, argon and other gases and gas mixtures*

In general between four and six experimental runs are performed at each (ρ, T) point. Each run fields a set of between 9 and 12 $\{\ln(t/t^{\circ}), \Delta T\}$ values and lasts approximately 1 s, thus keeping well inside the time for which convection effects become significant. The runs are carried out at a variety of positions of the switch S (see figure 11), which has the effect of varying the distribution of data points obtained on the $\ln(t/t^{\circ})$ axis, for the same final time. These runs may then be combined to give a larger set of $\{\ln(t/t^{\circ}), \Delta T\}$ data points up to $12n$, where n is the number of runs. Alternatively the runs can be analysed by averaging the individual thermal conductivity values obtained by fitting the set of $\{\ln(t/t^{\circ}), \Delta T\}$ values for each switch position. The latter method was found to give identical results to the more lengthy procedure of analysing the combined $\{\ln(t/t^{\circ}, \Delta T)\}$ points for a group of runs. The pressure, bath temperature and the times at which the bridge is in balance are logged automatically. For each isotherm a number of tests are also carried out to ensure that the apparatus is functioning correctly. Runs are done at increasingly longer times at both the high- and low-density ends of each isotherm, until significant convection is observed (by nonlinearity of the plot of $\{\ln(t/t^{\circ}), \Delta T\}$ at long times). This gives confidence in the final time of about one second for the measurement runs.

Each run is analysed automatically and immediately on completion, by the desk-top controller (Hewlett Packard 9836S). Two other input parameters are required at each density, namely the density of the gas at the reference temperature, and the specific heat capacity of the gas at constant pressure. These are obtained from various international tables or the best source available.

The dependence of thermal conductivity on wire-heating current is also checked. As the mean temperature rise of the experiment increases with bridge voltage it is important that the nominal thermal conductivity (the thermal conductivity corrected to some nominal temperature) does not change unduly. If this is done it is found that the thermal conductivities are identical to within their mutual uncertainties.

A further check is performed from time to time. The intercepts of the final linear least-squares fit of runs at the same (ρ, T) point are plotted against the heat generated per unit length of the wire. The intercept of this plot should be close to zero if the apparatus is functioning correctly. Figure 23 shows a typical plot for argon at 350 K, where this is the case.

At each temperature, the wire resistances at the equilibrium conditions are required. These are obtained by using the Wheatstone bridge manually in the steady-state mode as follows. A small voltage is applied across the bridge, with the switch number 1 in the S network closed, switch Q closed and the R network out of circuit (see figure 11). The bridge in this configuration is just a simple Wheatstone bridge with an effective resistance of 1 kΩ in each of the reference arms. Each wire is connected in turn to the long-wire terminals, the short-wire terminals having been shorted out with a copper link. The bridge is balanced manually by adjusting the resistors R_1 and R_2 until both HXOV indicator lights are lit with equal intensity. The measurements are repeated at a number of bridge voltages usually 2, 1.5, 1.0 and 0.5 V. Measured resistances are plotted against power and the zero-power intercept gives the true resistance at the bath temperature. In practice the balance points are determined from a set of two readings obtained by noting the resistances of R_1 and R_2 as the bridge comes into balance either side of zero. In other words as HXOV just changes from red to green and vice versa. The

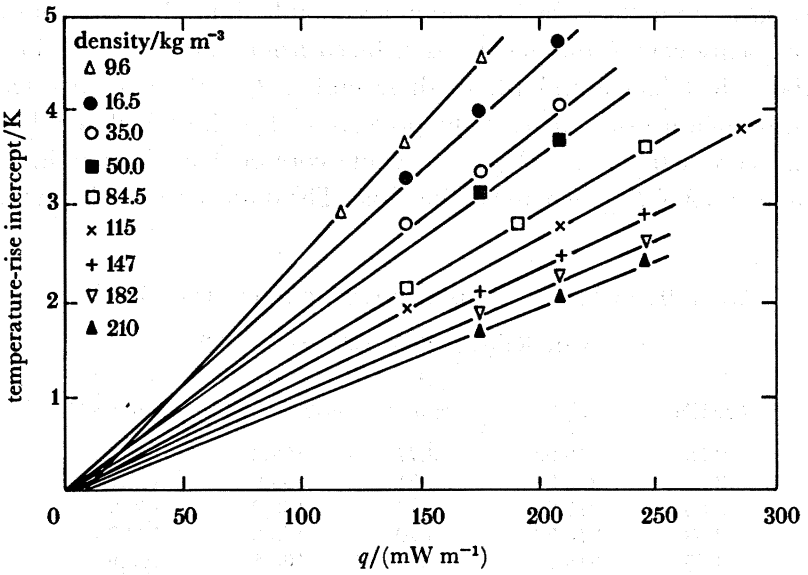

FIGURE 23. Variation of intercept of temperature rise with heat dissipation for Ar at 350 K and various densities. Symbols for densities: △, 9.6; ●, 16.5; ○, 35.0; ■, 50.0; □, 84.5; ×, 115; +, 147; ▽, 182; ▲, 210 kg m^{-3}.

mean of these two readings is taken to give the balance point of the bridge. It is important that the thermal electromotive forces across the bridge are compensated for, by adjusting the comparator offset, and checked at each voltage; otherwise the plot of resistance against power will not be a straight line.

At each density the reference temperature of the runs will be slightly different, thus it is necessary to correct the thermal conductivity to some nominal temperature for correlation purposes; this is done by means of the following equation:

$$\lambda(T_{\mathrm{nom}},\rho_{\mathrm{r}}) = \lambda(T_{\mathrm{r}},\rho_{\mathrm{r}}) + \{\partial\lambda(T,\rho_{\mathrm{r}})/\partial T\}_{T_{\mathrm{nom}}}(T_{\mathrm{nom}} - T_{\mathrm{r}}), \tag{7.1}$$

where T_{nom} is the chosen nominal temperature and T_{r} the measured reference temperature. In some cases it can be assumed that the temperature derivative of the thermal conductivity is density independent and the zero-density value used. This is a good approximation because the size of the correction is never greater than 0.5 % of $\lambda(T_{\mathrm{r}},\rho_{\mathrm{r}})$. However, near the critical region, where thermal conductivity is a strong function of both density and temperature, values of the derivatives from previous correlations are used.

Two gases, argon and helium, were chosen to test the performance of the apparatus. Firstly, because their thermal conductivities at zero density can be established from their viscosities using rigorous kinetic theory, and secondly, because they cover a wide span of thermal conductivity (the thermal conductivity of helium is approximately an order of magnitude greater than that of argon).

Two other input parameters are required at each state point, namely the density of the fluid at the reference temperature and equilibrium pressure of the run, and the specific heat capacity of the fluid at constant pressure. These were obtained from various international tables (Angus *et al.* 1972, 1977). The results for argon have been obtained over a long period with many different sets of wires and are summarized in table 11 at the end of this section, with other data from the apparatus.

The results for helium were obtained on two different wire sets at two temperatures 315 and

378 K and at pressures up to 25 MPa. To obtain acceptable times that were not too short, the maximum heat capacity correction factor was reduced from 1.005 to 1.001 for all runs. The results are tabulated in tables 9 and 10. In these tables, T_r is the reference temperature or average temperature of a measurement, P the pressure and ρ_r the calculated density, λ_r is the measured thermal conductivity and λ_{nom}, the value corrected to the nominal temperature T_{nom} from the value of $(\partial\lambda/\partial T)$ given above the table. The data were fitted to a linear equation

TABLE 9. THERMAL CONDUCTIVITY OF HELIUM AT 315 K

(T_{nom} = 315 K; $(\partial\lambda/\partial T)$ = 0.30 mW m^{-1} K^{-2}.)

P/MPa	T_r/K	ρ_r / kg m^{-3}	λ_r / mW m^{-1} K^{-2}	λ_{nom} / mW m^{-1} K^{-2}
2.53	315.93	3.77	163.8	163.5
3.00	315.84	4.51	163.0	162.7
3.65	315.85	5.47	163.2	162.9
3.83	315.76	5.70	163.0	162.7
4.65	315.77	6.95	163.8	163.6
5.66	315.54	8.42	163.7	163.6
6.65	315.48	9.85	163.4	163.3
7.71	315.43	11.37	164.3	164.1
8.50	315.31	12.50	164.2	164.1
9.65	315.29	14.13	165.0	164.9
10.30	315.23	15.03	164.8	164.7
11.70	315.00	16.96	165.3	165.3
13.15	314.95	18.96	166.1	166.1
14.80	314.86	21.23	166.3	166.3
17.25	314.63	24.49	166.7	166.9
19.20	314.63	27.06	167.9	168.1
19.95	314.33	28.08	167.9	168.1
21.35	314.28	29.88	169.1	169.4
22.80	314.26	31.71	169.3	169.6

TABLE 10. THERMAL CONDUCTIVITY OF HELIUM AT 378 K

(T_{nom} = 378 K; $(\partial\lambda/\partial T)$ = 0.29 mW m^{-1} K^{-2}.)

P/MPa	T_r/K	ρ_r / kg m^{-3}	λ_r / mW m^{-1} K^{-2}	λ_{nom} / mW m^{-1} K^{-1}
2.00	378.88	2.52	182.9	182.7
3.00	378.75	3.77	183.2	183.0
3.97	378.57	4.97	183.7	183.6
4.98	378.50	6.21	184.2	184.0
5.98	378.97	7.42	184.5	184.3
7.00	378.70	8.67	184.7	184.6
8.95	378.44	11.02	185.8	185.7
10.85	378.20	13.07	186.3	186.3
13.03	378.04	15.26	186.8	186.8
14.95	377.95	18.02	187.6	187.6
17.00	377.99	20.01	187.9	187.9
19.00	378.21	22.35	188.6	188.5
21.00	378.16	24.67	189.2	189.2
23.00	378.10	26.75	189.7	189.7
25.00	378.06	29.21	190.5	190.5

PHILOSOPHICAL TRANSACTIONS OF THE ROYAL SOCIETY A MATHEMATICAL, PHYSICAL & ENGINEERING SCIENCES

in the density. The coefficients a_0 and a_1, which best represent the data and are significant at the 95% confidence level, are shown in table 11.

The results for other gases and gas mixtures that have been studied by using this apparatus are given in the form of coefficients for the density polynomial in table 12. These coefficients were obtained by fitting data which has been published previously.

TABLE 11. HELIUM THERMAL CONDUCTIVITY POLYNOMIAL COEFFICIENTS

(From the correlation equation $\lambda = a_0 + a_1\rho$.)

T_{nom}/K	a_0 / mW m^{-1} K^{-1}	a_1 / mW m^2 K^{-1} kg^{-1}
315	161.2	0.253
378	182.2	0.287

TABLE 12. COEFFICIENTS OF THE CORRELATION EQUATION $\lambda = a_0 + a_1\rho + a_2\rho^2 + a_3\rho^3$ FOR DATA OBTAINED WITH LINE APPARATUS

	ρ_{max} / kg m^{-3}	T / K	$10^3 a_0$ / W m^{-1} K^{-1}	$10^6 a_1$ / W m^2 kg^{-1}	$10^9 a_2$ / W m^5 K^{-1} kg^{-2}	$10^{12} a_3$ / W m^8 K^{-1} kg^{-3}
He	32	315	161.2	253	0	0
He	29	378	182.2	287	0	0
Ar	236	313	18.41	20.08	31.9	0
Ar	211	350	20.25	22.40	21.9	0
Ar	223	375	21.42	22.49	22.2	0
Ar	264	427	23.74	20.62	29.7	0
Ar	129	470	25.54	20.34	37.9	0
H_2	15	311	192.10	1085	0	0
H_2	13	343	207.16	1049	0	0
H_2	13	385	225.18	1032	0	0
N_2	221	345	29.07	35.5	87.1	0
N_2	206	388	32.02	33.6	94.9	0
N_2	201	430	34.80	33.8	92.8	0
N_2	172	470	37.55	34.6	97.4	0
CO_2	145	302	16.91	20.58	271.2	−119.2
CO_2	595	316	19.65	45.51	696.0	−794.2
CO_2	711	348	20.10	33.17	31.36	−35.88
CO_2	553	380	23.17	25.98	131.2	−95.8
CO_2	457	430	27.36	25.05	105.0	−64.4
CO_2	396	470	31.03	20.52	111.8	−71.0
air	252	312	27.12	33.72	76.8	0
air	197	373	31.46	32.97	76.9	0
N_2/CO_2 ($X_{N_2} = 0.381$)	320	320	21.56	24.66	194.2	−207.8
N_2/CO_2 ($X_{N_2} = 0.166$)	428	380	24.54	25.65	126.4	−84.1
N_2/CO_2 ($X_{N_2} = 0.412$)	319	380	22.68	22.68	146.4	−120.4
N_2/CO_2 ($X_{N_2} = 0.708$)	240	380	21.23	21.23	177.4	−215.5
N_2/CO_2 ($X_{N_2} = 0.392$)	281	430	19.07	19.07	145.6	−124.1
N_2/CO_2 ($X_{N_2} = 0.582$)	261	470	34.54	20.72	123.2	0

(*b*) *Assessment of accuracy of the results*

To assess the absolute accuracy of the measurements we use the exact result of kinetic theory of dilute monatomic gases. The Chapman–Enskog first approximation to the Eucken factor $[f]_1$, is given by

$$[f]_1 = \{\lambda_0/\eta_0 c_v^0 F(T^*)\} = 2.500, \tag{7.2}$$

where λ_0 is the experimental value of thermal conductivity extrapolated to zero density, η_0 the experimental value of viscosity at zero density, c_v^0 the heat capacity at constant volume and $F(T^*)$ is a correction function that is given by (7.3) below, which is dependent on the form of the intermolecular potential, and has a value close to unity. Recent absolute measurements (Kestin *et al.* 1971) of the zero-density viscosity of the monatomic gases are reported to be accurate to within $\pm 0.2\,\%$; c_v^0 and $F(T^*)$ are also known to a fairly high accuracy. The value of c_v^0 for both He and Ar at these temperatures is given by $12.47\ \mathrm{J\ K^{-1}\ mol^{-1}}$.

The experimental data at each temperature are extrapolated to zero density by using a procedure of fitting to a polynomial with a successively increasing number of experimental points from low density upwards. Such a procedure was first used for obtaining second virial coefficients and has been described previously (Michels *et al.* 1960). The values obtained, which represent our experimental results for the zero-density thermal conductivity of He and Ar at various temperatures are given in the fifth column of table 13. The extrapolated zero-density

TABLE 13. EUCKEN FACTOR FOR HELIUM AND ARGON

gas	T/K	$F(T^*)$	η_0^+ / μ Pa s	λ_0 / mW m^{-1} K^{-1}	Eucken factor f_1	deviation ideal (%)
Ar	313	1.0010	23.58	18.38	2.499	−0.04
	350	1.0012	25.90	20.23	2.502	+0.08
	375	1.0014	27.41	21.40	2.499	−0.04
	427	1.0020	30.33	23.65	2.493	−0.28
	470	1.0028	32.64	25.44	2.490	−0.40
He	315	1.0045	20.60	161.2	2.500	0.00
	378	1.0046	23.41	182.2	2.478	−0.52

value is then substituted into (7.2). Table 13 shows the result of applying this procedure to argon and helium respectively. Values for $F(T^*)$ were derived for the Leonard Jones 12–6 potential function using values of ϵ/k obtained from the extended law of corresponding states described by Kestin *et al.* (1972). An analytic expression (Watson 1971) for $F(T^*)$ to the third approximation of Chapman and Enskog is

$$F(T^*) = f_\lambda^{(3)}/f_\eta^{(3)} = 1 + 0.0045\{1 - \exp\tfrac{1}{4}(1 - T^*)\}, \tag{7.3}$$

where $f_\lambda^{(3)}$ and $f_\eta^{(3)}$ are the Chapman–Enskog third-order correction terms for the thermal conductivity and viscosity calculated for the Leonard Jones 12–6 potential, and T^* is a reduced temperature defined by

$$T^* = T/(\epsilon/k), \tag{7.4}$$

where ϵ is the Leonard Jones parameter for the gas and k_B is Boltzmann's constant.

Table 13 shows that the present data confirm the expression (7.2) within an uncertainty smaller than or equal to $\pm 0.2\,\%$, except for the highest two temperatures for argon and the

378 K isotherm for helium. As far as the argon results go, it is possible that both (*a*) the estimate of $F(T^*)$ with the Leonard Jones potential at $T^* \approx 3$ is somewhat inaccurate, and (*b*) the systematic errors of measurement are greater at the higher temperatures.

The marked deviation of the 378 K Eucken value for helium can be ascribed to the viscosity values of Watson (1971) that, in the light of new data on helium, is thought to be high by about 0.3% at 378 K. This would make the Eucken value 2.495, only a -0.2% deviation from the ideal value and in line with the error tolerances of the other measurements. We can therefore judge the values of the zero density thermal conductivity to be accurate to within $\pm 0.25\%$.

We may conclude that the transient hot-wire apparatus described here has been shown to give excellent results over the temperature range 300–470 K and in the pressure range 0–25 MPa. The precision of measurement is some 0.1%, and values of the Eucken factors deduced from measurements on the two monatomic gases, argon and helium, agree to within $\pm 0.40\%$ of the theoretical value over the range of temperatures of the tests. The absolute uncertainty in the measurements over the whole range of operation is estimated to be within $\pm 0.5\%$.

We gratefully acknowledge the help given to us by Professor W. A. Wakeham of the Chemical Engineering Department, Imperial College, London. Professor Wakeham was involved as a consultant in the original design of the apparatus and continuously throughout the work. We thank Professor P. Gray for encouragement in this project and for criticisms of the manuscript. This work is supported by the Process Plant Advisory Committee of the Department of Trade and Industry. It is published with permission of the Director of the National Engineering Laboratory, East Kilbride.

References

Alloush, A., Gosney, W. B. & Wakeham, W. A. 1982 A transient hot-wire instrument for thermal conductivity measurements in electrically conducting liquids at elevated temperatures. *Int. J. Thermophys.* **3**, 225–236.

Andersson, P. & Backström, G. 1976 Instrument for measuring the thermal conductivity by the transient hot-wire technique. *Rev. scient. Instrum.* **47**, 205–209.

Angus, S. & Armstrong, B. (compilers) 1972 In *Argon – International tables of the fluid state*. London: Butterworths, for the International Union of Pure & Applied Chemistry.

Angus, S. & De Reuck, K. M. (compilers) 1977 In *Helium. International thermodynamic tables of the fluid state – 4*. Oxford: Pergamon Press, for the International Union of Pure & Applied Chemistry.

Assael, M., De Castro, C. A. N. & Wakeham, W. A. 1978 The estimation of physical properies of fluids. Part 2. The economic advantages of accurate transport property data. *Proc. Chempor '78*, paper 16.1. Braga: University of Mhino.

Assael, M. J. & Wakeham, W. A. 1980 The thermal conductivity of mixtures of hydrogen with the monatomic gases. *Ber. BunsenGes. phys. Chem.* **84**, 840–847.

Assael, M. J. & Wakeham, W. A. 1981 Thermal conductivity of four polyatomic gases. *J. chem. Soc. Faraday Trans.* I **77**, 697–707.

Assael, M. J., Dix, M., Lucas, A. & Wakeham, W. A. 1981 Absolute determination of the thermal conductivity of the noble gases and two of their binary mixtures as a function of density. *J. chem. Soc. Faraday Trans.* I **77**, 439–464.

Baryshev, V. P., Artamonov, S. D. & Geller, V. Z. 1980 The thermal conductivity of Freon-218. *J. engng Phys. SSSR* **38**, 147–151.

Blackwell, J. H. 1956 The axial flow error in the thermal conductivity probe. *Can. J. Phys.* **34**, 412–429.

Bootle, C. M., Ballantyne, J. C. & Roberts, R. T. 1984 Thermal conductivity measurements (in particular oils and fats) by means of an improved transient hot-wire technique. *British Food Manuf. Ind. Res. Assoc.* report M2. Leatherhead, Surrey, U.K.

Briggs, D. G. 1965 The measurement of the thermal conductivities of gases by a transient method. Ph.D. thesis. University of Minnesota, U.S.A.

PHILOSOPHICAL TRANSACTIONS OF THE ROYAL SOCIETY A MATHEMATICAL, PHYSICAL & ENGINEERING SCIENCES

Calado, J. C. G., Fareleira, J. M. N. A., De Castro, C. A. N. & Wakeham, W. A. 1983 Thermal conductivity of five hydrocarbons along the saturation line. *Int. J. Thermophys.* **4**, 193–208.

Carreker, R. P. Jr 1950 Plastic flow of platinum wires. *J. appl. Phys.* **21**, 1289–1296.

Carslaw, H. S. & Jaeger, J. C. 1959 In *Conduction of heat in solids* 2nd edn. Oxford: Clarendon Press.

Ciochina, A. & Vilcu, R. 1983 Transient hot-wire method for absolute and simultaneous measurement of thermal conductivity and thermal diffusivity of fluids. *Revue roum. Chim.* **28**, 795–804.

Clifford, A. A., Fleeter, R., Kestin, J. & Wakeham, W. A. 1979*a* Thermal conductivity of some mixtures of monatomic gases at room temperature and at pressures up to 15 MPa. *Physica* A **98**, 467–490.

Clifford, A. A., Fleeter, R. D., Kestin, J. & Wakeham, W. A. 1980*a* Thermal conductivity of mixtures of H_2 and He at 27.5 °C and pressures up to 14 MPa. *Ber. BunsenGes. phys. Chem.* **84**, 18–22.

Clifford, A. A., Gray, P., Johns, A. I., Scott, A. C. & Watson, J. T. R. 1981 Thermal conductivities of argon, nitrogen and hydrogen between 300 and 400 K and up to 25 MPa. *J. chem. Soc. Faraday Trans.* I **77**, 2679–2691.

Clifford, A. A., Kestin, J. & Wakeham, W. A. 1979*b* Thermal conductivities of nitrogen, carbon dioxide and methane at room temperature and at pressures up to 35 MPa. *Physica* A **97**, 237–295.

Clifford, A. A., Kestin, J. & Wakeham, W. A. 1980*b* A further contribution to the theory of the transient hot-wire technique for thermal conductivity measurements. *Physica* A **100**, 370–374.

Clifford, A. A., Kestin, J. & Wakeham, W. A. 1980*c* Thermal conductivity of hydrogen, deuterium and their mixtures near room temperature within the pressure range 2–36 MPa. *Ber. BunsenGes. phys. Chem.* **84**, 9–17.

Cousins, L. B. & Butterworth, D. 1979 The needs of industry for transport property data for heat exchanger design. In *Symp. on Transport Properties of Fluids and Fluid Mixtures. Their Measurement, Estimation, Correlation and Use*, paper no. 23. East Kilbride, Glasgow, U.K.: National Engineering Laboratory.

de Castro, C. A. N. 1977 Thermal conductivity measurement of liquid hydrocarbons by the hot-wire method (in Portuguese). Ph.D. thesis, Instituto Superior Tecnico, Lisbon.

de Castro, C. A. N. & Roder, H. M. 1981 Absolute determination of the thermal conductivity of argon at room temperature and pressures up to 68 MPa. *J. Res. natn. Bur. Stand.* **86**, 293–307.

de Castro, C. A. N., Calado, J. C. G. & Wakeham, W. A. 1976 An apparatus to measure thermal conductivities of liquids. *J. Phys.* E **9**, 1073–1080.

de Castro, C. A. N., Calado, J. C. G. & Wakeham, W. A. 1977 Absolute measurements of the thermal conductivity of liquids using the transient hot-wire technique. In *7th Symp. Thermophys. Properties*. Gaithersburg, Maryland: National Bureau of Standards.

de Castro, C. A. N., Calado, J. C. G. & Wakeham, W. A. 1979 Thermal conductivity of organic liquids measured by a transient hot-wire technique. *High Temp. High Press.* **11**, 551–559.

de Castro, C. A. N., Li, S. F. Y., Maitland, G. C. & Wakeham, W. A. 1983 Thermal conductivity of toluene in the temperature range 35–90 °C at pressures up to 600 mPa. *Int. J. Thermophys.* **4**, 311–328.

de Castro, C. A. N., Wakeham, W. A. & Calado, J. C. G. 1975 Thermal conductivity measurements of n-heptane along the saturation line by the transient hot-wire technique. *Chempor '78*. Instituto Superior Tecnico, Lisbon, Portugal.

de Groot, J. J., Kestin, J. & Sookiazian, H. 1974 An instrument to measure the thermal conductivity of gases. *Physica* **75**, 454–482.

de Groot, J. J., Kestin, J., Sookiazian, H. & Wakeham, W. A. 1978 The thermal conductivity of four monatomic gases as a function of density near room temperature. *Physica* A **92**, 117–145.

Dietz, F. J., de Groot, J. J. & Franck, E. U. 1980 High pressure thermal conductivity measurements of water with a.c. and d.c. transient hot-wire methods. In *Water and Steam, Their Prop. and Curr. Ind. Applic.*, Proc. 9th Conf. on Props. of Steam, Technical University, Munich. Oxford: Pergamon Press.

Falcao, A. F. O. 1967 A transient hot-wire method for the determination of the thermal conductivity of liquids. *Rev. port Quim.* **9**, 139–146.

Fareleira, J. M. N. A., Li, S. F. Y., Maitland, G. C. & Wakeham, W. A. 1984 Thermal conductivity of two branched alkanes in the temperature range 36–88 °C at pressures up to 0.6 GPa. *High Temp. High Press.* **16**, 427–434.

Fischer, J. 1939 Thermal conductivity measurement by the transient hot-wire method. *Annln Phys.* **34**, 669–688.

Fleeter, R., Kestin, J. & Wakeham, W. A. 1980 The thermal conductivity of three polyatomic gases and air at 27.5 °C and pressures up to 36 MPa. *Physica* A **103**, 521–543.

Fleeter, R., Kestin, J., Nagasaka, Y., Shankland, I. R. & Wakeham, W. A. 1982 The thermal conductivity of mixtures of methane with argon and neon. *Physica* A **111**, 404–423.

Fleeter, R., Kestin, J., Paul, R. & Wakeham, W. A. 1981*a* The thermal conductivity of mixtures of nitrogen with four noble gases at room temperature. *Physica* A **108**, 371–401.

Fleeter, R., Kestin, J., Paul, R. & Wakeham, W. A. 1981*b* The thermal conductivity of a binary mixture of helium and methane at 27.5 °C and at pressures up to 13 MPa. *Ber. BunsenGes. phys. Chem.* **85**, 215–220.

Friend, D. G. & Roder, H. M. 1985 Thermal conductivity enhancement near the liquid-vapour critical line of binary methane–ethane mixtures. *Phys. Rev.* A **32**, 1941.

Gillam, D. G., Romben, L., Nissen, H. & Lamm, O. 1955 Accurate determination of thermal conductivities. *Acta chem. scand.* **9**, 641–656.

PHILOSOPHICAL TRANSACTIONS OF THE ROYAL SOCIETY A MATHEMATICAL, PHYSICAL & ENGINEERING SCIENCES

Glatzmaier, G. C. & Ramirez, W. F. 1985 Simultaneous measurement of thermal conductivity and thermal diffusivity of unconsolidated materials by the transient hot-wire method. *Rev. scient. Instrum.* **56**, 1394–1398.

Goldstein, R. J. & Briggs, D. G. 1964 Transient free convection about vertical plates and circular cylinders. *Trans. Am. Soc. Mech. Engrs* C **86**, 490–500.

Haarman, J. W. 1969 An accurate method for the determination of the thermal conductivity coefficient of gases (non-stationary wire method). Ph.D. thesis, Technische Hogeschool, Delft.

Haarman, J. W. 1971 A contribution to the theory of the transient hot-wire method. *Physica* **52**, 605–619.

Haran, E. A. & Wakeham, W. A. 1982 A transient hot-wire cell for thermal conductivity measurements over a wide temperature range. *J. Phys.* E **15**, 839–842.

Haran, E. N., Maitland, G. C., Mustafa, M. & Wakeham, W. A. 1983 The thermal conductivity of argon, nitrogen and carbon monoxide in the temperature range 300–430 K at pressures up to 10 MPa. *Ber. BunsenGes. phys. Chem.* **87**, 657–663.

Healy, J. J., de Groot, J. J. & Kestin, J. 1976 The theory of the transient hot-wire method for measuring thermal conductivity. *Physica* C **82**, 392–408.

Hirschfelder, J. O., Curtiss, C. F. & Bird, R. B. 1954 In *Molecular theory of gases and liquids*. New York: John Wiley.

Horrocks, J. K. & McLaughlin, E. 1963 Non-steady state measurements of the thermal conductivity of liquid polyphenols. *Proc. R. Soc. Lond.* A **273**, 259–274.

Hoshi, M., Omotani, T. & Nagashima, A. 1981 Transient method to measure the thermal conductivity of high temperature melts using a liquid metal probe. *Rev. scient. Instrum.* **52**, 755–758.

Imaishi, N. & Kestin, J. 1984*a* Thermal conductivity of methane with carbon monoxide. *Physica* A **126**, 301–307.

Imaishi, N. & Kestin, J. 1984*b* Thermal conductivity of three noble gases with carbon monoxide. *Physica* A **126**, 98–115.

Imaishi, N., Kestin, J. & Paul, R. 1985 Thermal conductivity of carbon tetrafluoride with argon and helium. *Int. J. Thermophys.* **6**, 3–20.

Imaishi, N., Kestin, J. & Wakeham, W. A. 1984 Thermal conductivity of two binary mixtures of gases of equal molecular weight. *Physica* A **123**, 50–71.

Johns, A. I., Rashid, S., Watson, J. T. R. & Clifford, A. A. 1986 Thermal conductivity of argon, nitrogen and carbon dioxide at elevated temperatures and pressures. *J. chem. Soc. Faraday Trans.* I **82**, 2235–2246.

Johns, A. I., Rashid, S., Rowan, L., Watson, J. T. R. & Clifford, A. A. 1988 Thermal conductivity of mixtures of nitrogen and carbon dioxide at elevated temperatures and pressures. *Int. J. Thermophys.* **9**, 3.

Johns, A. I., Scott, A. C., Watson, J. T. R., Ferguson, D. & Clifford, A. A. 1983 *An apparatus for measuring the thermal conductivity of gases by the transient hot-wire method*. NEL report no. 685. East Kilbride, Glasgow, U.K.: National Engineering Laboratory.

Julia, Y. H., Renaud, J. F., Ferrand, D. J. & Malbrunot, P. E. 1977 A device for automatic thermal conductivity measurements. *Rev. scient. Instrum.* **48**, 1654–1658.

Kashiwagi, H., Hashimoto, T., Tanaka, Y., Kubota, H. & Makita, T. 1982*a* Thermal conductivity and density of toluene in the temperature range 273–373 K at pressures up to 250 MPa. *Int. J. Thermophys.* **3**, 201–215.

Kashiwagi, H., Oishi, M., Tanaka, Y., Kubota, H. & Makita, T. 1982*b* Thermal conductivity of fourteen liquids in the temperature range 298–373 K. *Int. J. Thermophys.* **3**, 101–116.

Kawaguchi, N., Nagasaka, Y. & Nagashima, A. 1985 Fully automated apparatus to measure the thermal conductivity of liquids by the transient hot-wire method. *Rev. scient. Instrum.* **56**, 1788–1794.

Kestin, J., Nagasaka, Y. & Wakeham, W. A. 1982*a* The thermal conductivity of mixtures of nitrogen with methane. *Ber. BunsenGes. phys. Chem.* **86**, 632–636.

Kestin, J. & Imaishi, N. 1985 Thermal conductivity of sulphur hexafluoride. *Int. J. Thermophys.* **6**, 107–118.

Kestin, J., Nagasaka, Y. & Wakeham, W. A. 1982*b* The thermal conductivity of mixtures of hydrogen with nitrogen. *Ber. BunsenGes. phys. Chem.* **86**, 187.

Kestin, J., Nagasaka, Y. & Wakeham, W. A. 1982*c* The thermal conductivity of mixtures of carbon dioxide with three noble gases. *Physica* A **113**, 1–26.

Kestin, J., Paul, R., Clifford, A. A. & Wakeham, W. A. 1980 Absolute determination of the thermal conductivities of the noble gases at room temperature and at pressures up to 35 MPa. *Physica* A **100**, 349–369.

Kestin, J., Ro, S. T. & Nagasaka, Y. 1983 Thermal conductivities of mixtures of methane with carbon dioxide. *Ber. BunsenGes. phys. Chem.* **86**, 945–948.

Kestin, J., Ro, S. T. & Wakeham, W. A. 1971 Reference values of the viscosity of twelve gases at 25 °C. *Trans. Faraday Soc.* **67**, 2308–2313.

Kestin, J., Ro, S. T. & Wakeham, W. A. 1972 An extended law of corresponding states for the equilibrium and transport properties of the noble gases. *Physica* **58**, 165–211.

Kestin, J. J. & Wakeham, W. A. 1978 A contribution to the theory of the transient hot-wire technique for thermal conductivity measurements. *Physica* A **92**, 102–117.

Khalifa, H. E., Kestin, J. & Wakeham, W. A. 1979 The theory of the transient hot-wire method for measuring the thermal conductivity of gaseous mixtures. *Physica* A **97**, 273–287.

Kitazawa, N. & Nagashima, A. 1981 Measurement of thermal conductivity of liquids by a transient hot-wire method. 2. Measurement under high pressure. *Bull. J.S.M.E.* **24**, 374–379.

PHILOSOPHICAL TRANSACTIONS OF THE ROYAL SOCIETY A MATHEMATICAL, PHYSICAL & ENGINEERING SCIENCES

Knibbe, P. G. 1985 Simultaneous thermal conductivity and thermal diffusivity measurements. In *9th Int. Symp. on Thermophysical Properties*, 24–28 June 1985. Boulder, Colorado: National Bureau of Standards. (*Int. J. Thermophys.* **8**, 181–192 (1987).)

Li, S. F. Y., Maitland, G. C. & Wakeham, W. A. 1984*a* The thermal conductivity of n-hexane and n-octane at pressures up to 0.64 GPa in the temperature range 34–90 °C. *Ber. BunsenGes. phys. Chem.* **88**, 32–36.

Li, S. F. Y., Maitland, G. C. & Wakeham, W. A. 1984*b* Thermal conductivity of benzene and cyclohexane in the temperature range 36–90 °C at pressures up to 0.33 GPa. *Int. J. Thermophys.* **5**, 351–366.

Maitland, G. C., Mustafa, M., Ross, M., Trengove, R. D., Wakeham, W. A. & Zalaf, M. 1986 Transient hot-wire measurements of the thermal conductivity of gases at elevated temperatures. *Int. J. Thermophys.* **7**, 245–258.

Mani, N. 1971 Thermal conductivities of liquids by the transient hot-wire method. Ph.D. thesis, University of Calgary, Canada.

Mardolcar, U. V. & Wakeham, W. A. 1983 Thermal conductivity of carbon disulphide at pressures up to 500 MPa. *Int. J. Thermophys.* **4**, 1–10.

Mardolcar, U. V., de Castro, C. A. N. & Wakeham, W. A. 1986 Thermal conductivity of argon in the temperature range 107–427 K. *Int. J. Thermophys.* **7**, 259–272.

Mardolcar, U. V., Fareleira, J. M. N. A., de Castro, C. A. N. & Wakeham, W. A. 1985 Measurement of the thermal conductivity of argon: a test of the accuracy of the transient hot-wire method. *High Temp. High Press.* **17**, 469–476.

McLaughlin, E. & Pitman, J. F. T. 1971 Determination of the thermal conductivity of toluene; a proposed standard from 180–400 K by the transient hot-wire method. *Phil. Trans. R. Soc. Lond.* A **270**, 579–602.

Menashe, J. & Wakeham, W. A. 1981 Absolute measurements of the thermal conductivity of liquids at pressures up to 500 MPa. *Ber. BunsenGes. phys. Chem.* **85**, 340–347.

Menashe, J. & Wakeham, W. A. 1982*a* Effect of absorption of radiation on thermal conductivity measurements by the transient hot-wire technique. *Int. J. Heat Mass Transfer* **25**, 661–673.

Menashe, J. & Wakeham, W. A. 1982*b* Thermal conductivity of n-nonane and n-undecane at pressures up to 500 MPa in the temperature range 35–90 °C. *Ber. BunsenGes. phys. Chem.* **86**, 541–545.

Michels, A., Abels, J. C., Ten Seldam, C. A. & De Graff, W. 1960 Polynomial representation of experimental data: application to virial coefficients of gases. *Physica* **26**, 381–393.

Mustafa, M., Sage, M. & Wakeham, W. A. 1982 Thermal conductivity of n-tridecane at pressures up to 500 MPa in the temperature range 35–75 °C. *Int. J. Thermophys.* **3**, 217–224.

Nagasaka, Y. & Nagashima, A. 1981*a* Simultaneous measurement of the thermal conductivity and thermal diffusivity of liquids by the transient hot-wire method. *Rev. scient. Instrum.* **52**, 229–232.

Nagasaka, Y. & Nagashima, A. 1981*b* Precise measurements of the thermal conductivity of toluene and n-heptane by the absolute transient hot-wire method. *Ind. Engng Chem. Fundam.* **20**, 216–220.

Nagasaka, Y. & Nagashima, A. 1981*c* Absolute measurement of the thermal conductivity of electrically conducting liquids by the transient hot-wire method. *J. Phys.* E **14**, 1435–1441.

Nagasaka, Y., Kamimoto, M., Abe, Y. & Nagashima, A. 1986 Thermophysical property measurements on pentaerythritol and related storage materials II. Thermal conductivity by transient hot-wire. In *Proc. 1st. Asian Thermophysical Props Conf.* Bejing: China Academic Publishers.

Nagasaka, Y., Okada, H., Suzuki, J. & Nagashima. A. 1983 Absolute measurements of the thermal conductivity of aqueous NaCl solutions at pressures up to 40 MPa. *Ber. BunsenGes. phys. Chem.* **87**, 859–866.

Nagasaka, Y., Suzuki, J. & Nagashima. A. 1984 The thermal conductivity of aqueous KCl solutions at pressures up to 40 MPa. In *Proc. 10th Int. Conf. on Properties of Steam*, 2–7 September, paper IV–15, Moscow, U.S.S.R.

Omotani, T. & Nagashima, A. 1984 Thermal conductivity of molten salts, HTS and the $LiNO_3$–$NaNO_3$, system using a modified transient hot-wire method. *J. Chem. Engng Data* **29**, 1–3.

Omotani, T., Nagasaka, Y. & Nagashima, A. 1982 Measurement of thermal conductivities of KNO_3–$NaNO_3$ mixtures using a transient hot-wire method with a liquid metal in a capillary probe. *Int. J. Thermophys.* **3**, 17–26.

Palavra, A. M. F., Wakeham, W. A. & Zalaf, M. 1986 Thermal conductivity of carbon tetrachloride in the temperature range 310–364 K at pressures up to 0.22 GPa. *Int. J. Thermophys.* **6**, 427–438.

Parsons, J. R. & Mulligan, J. C. 1978 Measurement of the properties of liquids and gases using a transient hot-wire technique. *Rev. scient. Instrum.* **49**, 1460–1463.

Perkins, R. A. 1983 Development of a transient hot-wire apparatus to measure thermal conductivity of fluids at high temperatures and pressures. Ph.D. thesis, U.S. Colorado School of Mines.

Perkins, R. A., Mohammadi, S. S., McAllister, R., Graboski, M. S. & Sloan, E. D. 1981 New transient vertical hot-wire thermal conductivity instrument for fluids utilising a ramp power input. *J. Phys.* E **14**, 1279–1284.

Picot, J. J. 1969 Thermal conductivities of gases using the transient hot-wire method. *Can. J. chem. Engng* **47**, 17–19.

Prasad, R. C. & Venart, J. E. S. 1984 Thermal conductivity of ethane from 290–600 K at pressures up to 700 bar including the critical region. *Int. J. Thermophys.* **5**, 367–386.

Prasad, R. C., Mani, N. & Venart, J. E. S. 1984 Thermal conductivity of methane. *Int. J. Thermophys.* **5**, 265–280.

Richmond, J., Nilsson, O. & Sandberg, O. 1984 Thermal properties of some lubricants under pressure. *J. appl. Phys.* **56**, 2065–2067.

PHILOSOPHICAL TRANSACTIONS OF THE ROYAL SOCIETY A MATHEMATICAL, PHYSICAL & ENGINEERING SCIENCES

Riddle, J. R., Furukawa, G. T. & Plumb, H. H. 1972 In *Platinum resistance thermometry*. NBS Monogr. no. 126. Washington, D.C.: National Bureau of Standards.

Roder, H. M. 1981 Transient hot-wire thermal conductivity apparatus for fluids. *J. Res. natn. Bur. Stand.* **86**, 457–493.

Roder, H. M. 1982 The thermal conductivity of oxygen. *J. Res. natn. Bur. Stand.* **87**, 279–310.

Roder, H. M. 1984*a* Thermal conductivity of hydrogen for temperatures between 78 and 310 K with pressures to 70 MPa. *Int. J. Thermophys.* **5**, 323–350.

Roder, H. M. 1984*b* Thermal conductivity of para-hydrogen. *J. Chem. Engng Data* **29**, 382–386.

Roder, H. M. 1985 Thermal conductivity of methane for temperatures between 110 and 310 K with pressures to 70 MPa. *Int. J. Thermophys.* **6**, 119–142.

Roder, H. M. & de Castro, C. A. N. 1982 Thermal conductivity of liquid propane. *J. Chem. Engng Data* **27**, 12–16.

Roder, H. M. & de Castro, C. A. N. 1985 Thermal conductivity of ethane at temperatures between 110 and 325 K and pressures up to 70 MPa. *High Temp. High Press.* **17**, 453–460.

Roder, H. M. & Friend, D. G. 1986 Thermal conductivity of methane–ethane mixtures at temperatures between 140 and 330 K at pressures up to 70 MPa. *Int. J. Thermophys.* **6**, 607–618.

Saito, A. & Venart, J. E. S. 1978 Radiation effects with the transient line source measurement of fluid thermal conductivity. In *Sixth Int. Heat Transfer Conf.*, Toronto, Canada, August 1978, pp. 79–84. Canada: Hemisphere.

Scott, A. C., Johns, A. I., Watson, J. T. R. & Clifford, A. A. 1981 Thermal conductivity of air in the temperature range 312–373 K and 0.1–24 MPa. *Int. J. Thermophys.* **2**, 103–114.

Scott, A. C., Johns, A. I., Watson, J. T. R. & Clifford, A. A. 1983 Thermal conductivity of carbon dioxide in the temperature range 300–348 K and pressures up to 25 MPa. *J. chem. Soc. Faraday Trans.* I **79**, 733–740.

Serbanescu, D., Vasu, Gh., Vilcu, R. & Ciochina, A. 1981 Transient hot-wire thermal conductivimeter for absolute measurements in fluids. *Revue roum. Chim.* **26**, 1047–1062.

Shpil'ran, E. E., Umanskii, A. S. & Gorshkov, Y. A. 1975 Non steady-state methods of measuring the thermal conductivity of gases (a review). *High Temp. High Press.* **7**, 361–393.

Smoluchowski, M. 1911*a* Some remarks on conduction of heat through rarified gases. *Phil. Mag.* **21**, 11–14.

Smoluchowski, M. 1911*b* Remarks on the theory of heat conduction in rarified gases and the resulting pressure forces. *Annln Phys. Chem.* **35**, 983–1004.

Song, Y. W. & Yu, J. L. 1984 An instrument for the rapid determination of thermal conductivity and diffusivity of liquids. *Kexue Tongbao* **29**, 974–978.

Sookiazian, H. 1977 Precise measurement of the thermal conductivity of gases by the transient hot-wire technique. Ph.D. thesis, Brown University, Providence, Rhode Island.

Stalhane, B. & Pyk, S. 1931 A new method for determining thermal conductivity. *Tek. Tidsskr.* **61**, 389.

Sutton, J. R. 1969 *References to experimental data on thermal conductivity of gas mixtures*. NEL report no. 409. East Kilbride, Glasgow, U.K.: National Engineering Laboratory.

Sutton, J. R. 1976 *References to experimental data on thermal conductivity of gas mixtures*. NEL report no. 612. East Kilbride, Glasgow, U.K.: National Engineering Laboratory.

Takizawa, S., Murata, H. & Nagashima, A. 1978 Measurement of the thermal conductivity of liquids by the transient hot-wire method I. Measurement at atmospheric pressure. *Bull. J.S.M.E.* **21**, 273–278.

Takizawa, S., Nagashima, A. & Tanishita, I. 1974 Thermal conductivity of water by the transient hot-wire method. In *Proc. 8th Conf. for the properties of Steam*, Giens, France, paper no. 2.6, pp. 245–254. France: Éditions Européennes Thermiques et Industries with the contribution of Délégation Générale à la Recherche Scientifique et Technique.

Trump, W. N., Luebke, H. W., Fowler, L. & Emery, E. M. 1977 Rapid measurement of liquid thermal conductivity by the transient hot-wire method. *Rev. scient. Instrum.* **48**, 47–51.

Tsymarnyi, V. A. & Potienko, N. F. 1976 Making allowance for thermal capacity of a heat source when measuring the coefficient of thermal conductivity by the non-stationary method. VINITI deposited paper 2291-74. [English transl. (LTS1951/76) NEL TT 2726. East Kilbride, Glasgow, U.K.: National Engineering Laboratory.]

Van der Held, E. F. M. & Van Drunen, F. G. 1949 Transient hot-wire thermal conductivity apparatus. *Physica* **15**, 865–881.

Venart, J. E. S. & Mani, N. 1975 Thermal conductivity of refrigerant-12 (300–600 K; 0.2–20 MPa). *Trans. Can. Soc. mech. Engrs* **3**, 1–9.

Venart, J. E. S., Prasad, R. C. & Stocker, D. G. 1980 Thermal conductivity of water and heavy water. Water and steam, their properties and current industrial applications. In *Proc. 9th Conf. on props. of steam*, Tech. Univ. Munich. Sept. 1979, pp. 392–406. Oxford: Pergamon Press.

Vilcu, R. & Ciochina, A. 1981 Absolute measurement of thermal conductivity and thermal diffusivity of liquids by the classical procedure of the transient hot-wire method. *Revue roum. Chim.* **26**, 527–537.

Vilcu, R., Ciochina, A. & Vasu, Gh. 1982 Absolute measurement of thermal conductivity and thermal diffusivity of gases by the classical transient hot-wire method. *Revue roum. Chim.* **27**, 313–323.

Wada, Y., Nagasaka, Y. & Nagashima. A. 1985 Measurements and correlation of the thermal conductivity of liquid n-paraffin hydrocarbons and their binary and ternary mixtures. *Int. J. Thermophys.* **6**, 251–266.

PHILOSOPHICAL TRANSACTIONS OF THE ROYAL SOCIETY A MATHEMATICAL, PHYSICAL & ENGINEERING SCIENCES

Wahl, A. M. 1963 *Mechanical springs*. New York: McGraw-Hill.

Wakeham, W. A. 1979 Fluid thermal conductivity measurements by the transient hot-wire technique. In *Symp. on Transport Properties of Fluids and Fluid Mixtures. Their Measurement, Estimation, Correlation and Use*, paper 1.1. East Kilbride, Glasgow, U.K.: National Engineering Laboratory.

Wakeham, W. A. 1986 Transport properties of polyatomic gases. *Int. J. Thermophys.* **7**, 1–17.

Watson, J. T. R. 1971 *Viscosity and thermal conductivity coefficients of the rare gases from 270–2000 K*. NEL report no. 488. East Kilbride, Glasgow, U.K.: National Engineering Laboratory.

Yata, J., Minamiyama, T. & Tanaka, S. 1984 Measurement of thermal conductivity of liquid fluorocarbons. *Int. J. Thermophys.* **5**, 209–218.

PHILOSOPHICAL TRANSACTIONS OF THE ROYAL SOCIETY A MATHEMATICAL, PHYSICAL & ENGINEERING SCIENCES

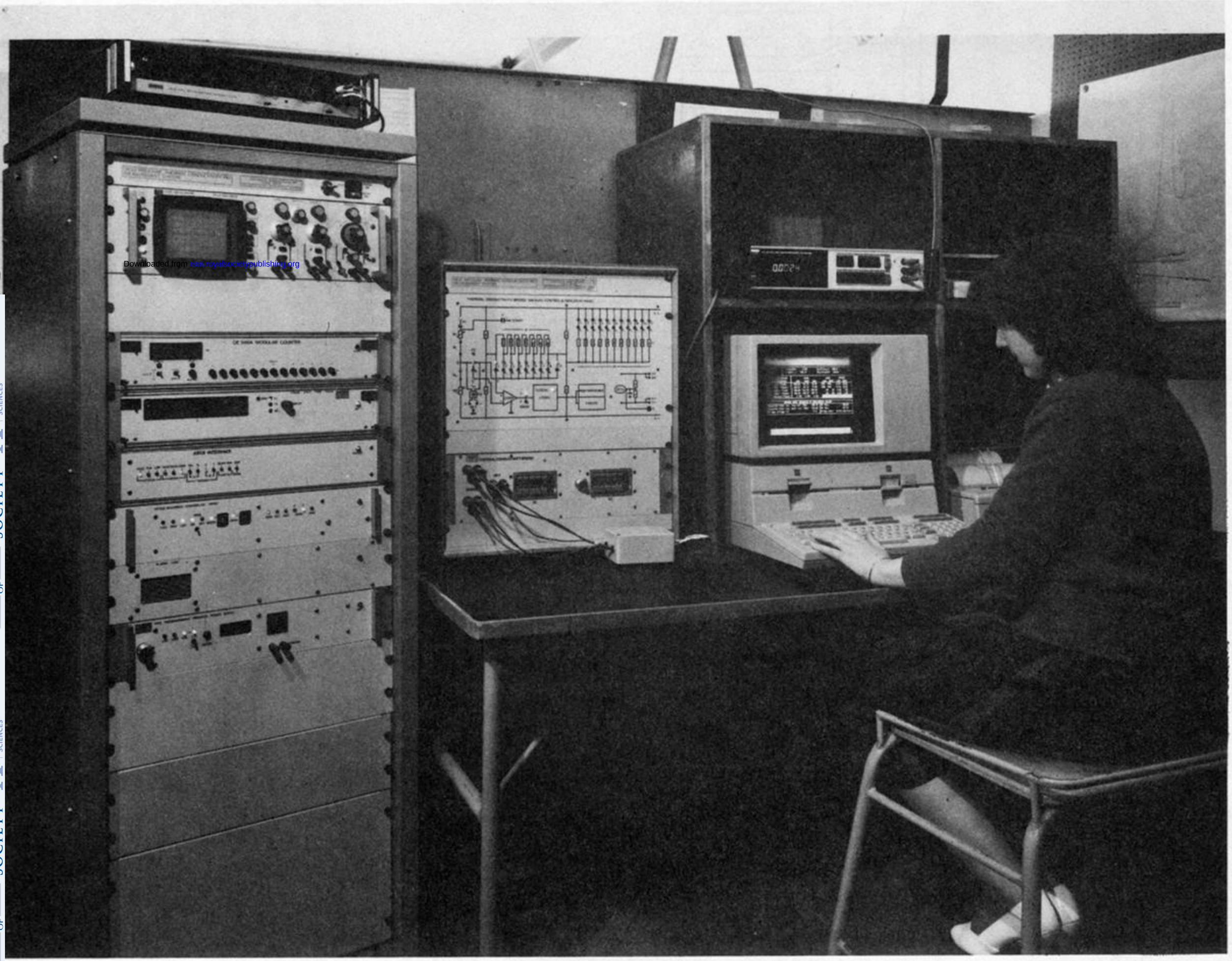

FIGURE 9. Instrument layout showing control computer and electronic equipment.

PHILOSOPHICAL TRANSACTIONS OF THE ROYAL SOCIETY A MATHEMATICAL, PHYSICAL & ENGINEERING SCIENCES